

# Syntheses and Structures of Iron(II) and Cobalt(II) Complexes of Substituted Tetra(pyrazolyl)lutidine Derivatives

Heidi Marie Tatlock  
*Marquette University*

---

## Recommended Citation

Tatlock, Heidi Marie, "Syntheses and Structures of Iron(II) and Cobalt(II) Complexes of Substituted Tetra(pyrazolyl)lutidine Derivatives" (2013). *Master's Theses (2009 -)*. 236.  
[https://epublications.marquette.edu/theses\\_open/236](https://epublications.marquette.edu/theses_open/236)

SYNTHESES AND STRUCTURES OF IRON(II) AND COBALT(II) COMPLEXES OF  
SUBSTITUTED TETRA(PYRAZOLYL)LUTIDINE DERIVATIVES

by

Heidi M. Tatlock

A Thesis Submitted to the Faculty of the Graduate School,  
Marquette University,  
in Partial Fulfillment of the Requirements for  
the Degree of Master of Science

Milwaukee, WI

December 2013

# ABSTRACT

## SYNTHESES AND STRUCTURES OF IRON(II) AND COBALT(II) COMPLEXES OF SUBSTITUTED TETRA(PYRAZOLYL)LUTIDINE DERIVATIVES

Heidi M. Tatlock

Marquette University, 2013

Pentadentate ligands provide stability to metal complexes as well as a binding site for substrates that make them exceptionally useful for studying reactions. They have been used in biomimetic studies, water splitting, and small molecule activation studies.

A series of six pentadentate ligands derived from  $\alpha,\alpha',\alpha'$ -tetra(pyrazolyl)lutidine,  $\text{pz}_4\text{lut}$ , with methyl substituents decorating the ligand periphery has been synthesized. These ligands were coordinated to  $\text{Fe}^{\text{II}}\text{Cl}$ , and the electronic and structural properties of the resulting complexes were studied in order to deduce the effects of methyl substitution at the 3-, 4-, and 5-positions of the pyrazolyl groups and at the methine positions. When analyzed via cyclic voltammetry, the resulting complexes exhibited oxidation waves between 0.95 V and 0.75 V. It was determined that the 4-pyrazole position controls electronic effects, and the 3-pyrazolyl position controls steric effects. Substitution at the methine positions favors a low-spin  $\text{Fe}^{\text{II}}$  complex. It is thought that adding bulkier groups to the methine positions may change the coordination environment of the resulting complex. An  $[\text{Fe}^{\text{III}}(\text{OH})(\text{pz}_4\text{depy})]$  complex ( $\text{pz}_4\text{depy} = \alpha,\alpha',\alpha'$ -tetra(pyrazolyl)diethylpyridine) could be capable of oxidizing hydrocarbons with BDE (bond dissociation enthalpy) values less than 93 kcal/mol.

A  $[\text{Co}^{\text{II}}(\text{H}_2\text{O})(\text{pz}_4\text{depy})]^{2+}$  complex was shown to be capable of water oxidation via a concerted proton-electron transfer (PCET) mechanism. This complex was compared to a similar WOC,  $[\text{Co}^{\text{II}}(\text{H}_2\text{O})(\text{PY5})]^{2+}$ , and found to react with water via a more favorable pathway. The BDFE(OH) (bond dissociation free energy of the OH bond) was also calculated via DFT calculations to be 76.7 kcal/mol, which is higher than that of  $[\text{Co}^{\text{II}}(\text{H}_2\text{O})(\text{PY5})]^{2+}$  by 5 kcal/mol. Further studies are needed to make sure that the catalytically active species is not  $\text{CoO}_x$  nanoparticles that may have formed in solution. The  $[\text{Co}^{\text{II}}(\text{H}_2\text{O})(\text{pz}_4\text{depy})]^{2+}$  complex is also thought to be capable of CH-activation reactions.

This thesis demonstrates the versatility of a new pentadentate ligand family for controlling the electronic and structural properties of transition metal complexes. The data reported herein may be used to select the appropriate complex to participate in CH-activation reactions.

## ACKNOWLEDGEMENTS

Heidi M. Tatlock

First and foremost, I would like to thank God the Father, Son, and Holy Spirit.

I would like to thank my undergraduate advisor, Dr. Kevin W. Glaeske at Wisconsin Lutheran College, for challenging me to go to graduate school. I would not have applied if it wasn't for his stories about the demanding trials and the thrill of finding something new.

I would like to thank my husband, Dave, for all of his love and support along the way. He is an amazing leader for our family.

I would like to thank my advisor, Dr. James R. Gardinier, for giving me this opportunity to work in his lab. His encouragement and advice were vital to my success. I would also like to thank Sarath Wanniarachchi for taking the time to show me how to use Schlenk methods and for being a good friend. Finally, I would like to thank Dr. Sergey Lindeman for his help with crystal structures.

## TABLE OF CONTENTS

ACKNOWLEDGEMENTS .....	i
LIST OF TABLES.....	iv
LIST OF FIGURES AND SCHEMES.....	v
CHAPTERS	
CHAPTER 1: INTRODUCTION.....	1
1-1 Introduction to Coordination Chemistry and Pentadentate Ligands.....	1
1-2 Pentadentate ligands that Support Transition Metal Complexes .....	3
1-3 Previously Studied pz <sub>4</sub> lut Transition Metal Complexes .....	5
CHAPTER 2: IRON(II) CHLORIDE COMPLEXES OF PZ <sup>R</sup> <sub>4</sub> LUT and PZ <sup>R</sup> <sub>4</sub> DEPY .....	7
2-1 Introduction .....	7
2-2 Synthesis .....	8
2-3 Crystallography.....	11
2-4 Results .....	14
2-5 Conclusions .....	29
CHAPTER 3: AQUACOBALT(II) COMPLEXES OF PZ <sup>R</sup> <sub>4</sub> DEPY .....	30
3-1 Introduction .....	30
3-2 Synthesis.....	31
3-3 Crystallographic Structure Determinations .....	33
3-4 Calculations .....	34
3-5 Results and Discussion .....	35
3-6 Conclusions.....	45
CHAPTER 4: CONCLUSIONS AND OUTLOOK.....	47
4-1 Conclusions.....	47

4-2 Future Directions.....	48
REFERENCES .....	49

## LIST OF TABLES

<b>Table 1-1:</b> Stability constants for various nickel (II) complexes .....	2
<b>Table 1-2:</b> Examples of four different classes of pentadentate ligands .....	4
<b>Table 2-1.</b> Crystallographic data for <b>5</b> ·MeOH at T=100 K and 296 K .....	12
<b>Table 2-2.</b> Crystallographic data collection and structure refinement for [CoCl(pz <sub>4</sub> depy)]Cl·MeOH, <b>7</b> ·MeOH at T=296 K and T=100 K .....	13
<b>Table 2-3.</b> Selected interatomic bond distances (Å), bond angles (°), and bond torsions (°) in <b>1-5</b> .....	18
<b>Table 3-1.</b> Crystallographic data collection and structure refinement for [ <b>2</b> ](ClO <sub>4</sub> ) and [ <b>2</b> ](OTs) <sub>2</sub> ·3H <sub>2</sub> O .....	33
<b>Table 3-2.</b> Comparison of calculated (M06/Def2-SV(P)) versus experimental bond distances and angles in [(PY5)Co <sup>II</sup> (H <sub>2</sub> O)] <sup>2+</sup> and [(pz <sub>4</sub> depy)Co <sup>II</sup> (H <sub>2</sub> O)] <sup>2+</sup> .....	34
<b>Table 3-3.</b> Selected structural parameters of the two dications in [Co(H <sub>2</sub> O)(pz <sub>4</sub> depy)](OTs) <sub>2</sub> ·3H <sub>2</sub> O, <b>2</b> ·3H <sub>2</sub> O .....	36
<b>Table 3-4.</b> Free energy (kcal/mol) of each species in Figure 3-5 .....	39
<b>Table 3-5.</b> Summary of SCF energies and thermochemical data from theoretical calculations for (L)Co <sup>n+</sup> (OH <sub>x</sub> ) where L=PY5 .....	39
<b>Table 3-6.</b> Summary of SCF energies and thermochemical data from theoretical calculations for (L)Co <sup>n+</sup> (OH <sub>x</sub> ) where L= pz <sub>4</sub> depy .....	39
<b>Table 3-7.</b> Main structural features in (M06/Def2-SV(P)) geometry- optimized [(L)Co(OH <sub>x</sub> )] <sup>z</sup> .....	40
<b>Table 4-1.</b> Predicted oxidation reactions of C-H bonds with [Fe <sup>III</sup> pz <sub>4</sub> depy(H <sub>2</sub> O)] <sup>3+</sup> as catalyst .....	47

## LIST OF FIGURES AND SCHEMES

<b>Scheme 2-1.</b> Preparation of $\text{pz}^{\text{R}}_4\text{lut}$ ligands described in this work .....	14
---	----

**Figure 2-1.** Top left: Structure of the cation in  $[\text{FeCl}(\text{pz}^*_4\text{lut})]\text{Cl}$  (**3**) shown with thermal ellipsoids at the 50% probability level; Top right: Overlay of all cation structures in **1** (green), **2** (orange), **3** (blue) and **4** (violet). Bottom: Space-filling representations for cations in **3** (left) and **1** (right) where the areas with potential steric interactions are highlighted by arrows .....

**Figure 2-2.** Left and middle: Views of the 100 K structure of the  $[\text{FeCl}(\text{pz}_4\text{depy})]^+$  cation; Right: Overlay of 296 K (red) and 100 K (black) structures .....

**Figure 2-3.** Structural depictions and overlays of  $[\text{CoCl}(\text{pz}_4\text{depy})](\text{Cl})\cdot\text{MeOH}$ , **7**·MeOH. Left: 296 K (red wireframe) and 100 K (blue wireframe) structures. Right: partial atom labeling of 100 K structure .....

**Figure 2-4.** Left: Overlay of cation structures in **1** (green) and **5** (red); Middle and right: Side views of space-filling representations of **5** and **1**, respectively, highlighting potential steric interactions in **5** .....

**Figure 2-5.** Main structural distortions for heteroscorpionate,  $\text{RCpz}_2\text{py}$ , fragments that occur upon binding metal cations of different size. R is H or an organic substituent while C-N and N-N represent the pyridyl and pyrazolyl rings, respectively .....

**Figure 2-6.** Calculated (blue, bottom) and observed (black, top) PXRD data for **5**·MeOH .....

**Figure 2-7.** Temperature dependence of the magnetic moment of **5** (red, higher trace) and **6** (black, lower trace) in MeOH .....

**Figure 2-8.** Photograph of samples complexes **1-6** .....

**Figure 2-9.** Left: Overlay of the d-d region of the spectrum of each **1** (green), **2** (orange), **3** (blue), and **4** (violet) in MeOH. Right: Overlay of electronic absorption spectrum of **1** (green), **5** (red) and of **6** (black) in MeOH .....

**Figure 2-10.** Cyclic voltammograms of the iron(II) chloride complexes of  $\text{pz}^{\text{R}}_4\text{lut}$  and  $\text{pz}^{\text{R}}_4\text{depy}$  in MeOH obtained at 100 mV/s with  $(\text{NBu}_4)(\text{HSO}_4)$  as the supporting electrolyte .....

**Scheme 3-1.** Metallation of  $[\text{Co}(\text{H}_2\text{O})_6](\text{OTs})_2$  with  $\text{pz}_4\text{depy}$  .....

**Figure 3-1.** View of the structure of  $[\text{2}](\text{ClO}_4)$  with partial atom labeling. The dication resides on a two-fold axis of rotation .....

**Figure 3-2.** View of the two dications in  $[\text{Co}(\text{H}_2\text{O})(\text{pz}_4\text{depy})](\text{OTs})_2\cdot 3\text{H}_2\text{O}$ , **2**· $3\text{H}_2\text{O}$  .....



<b>Figure 3-3.</b> Comparison of dicationic structures of <b>1</b> (green) and <b>2</b> (red) where atoms of axial pyridine rings are overlaid to highlight the more idealized octahedral geometry of <b>2</b> .....	37
<b>Figure 3-4.</b> $\beta$ -HOMOs of $[(L)Co^{II}(OH)]^+$ (bottom) and HOMO of $[(L)Co^{III}(OH)]^{2+}$ (top) for L = PY5 (left) and pz <sub>4</sub> depy (right).....	38
<b>Figure 3-5.</b> Comparison of Pourbaix diagrams of $[(PY5)Co(OH_2)]^{2+}$ , <b>1</b> versus $[(pz_4depy)Co(OH_2)]^{2+}$ , <b>2</b> .....	41
<b>Scheme 3-2.</b> Thermodynamic square-scheme cycle used to calculate the bond dissociation free energy (BDFE) associated with the $[LCo^{II}(H_2O)]/[LCo^{III}(OH)]^{2+}$ event .....	42
<b>Figure 3-6.</b> Cyclic voltammograms of <b>1</b> and <b>2</b> (0.5 mM) recorded in 0.1 M KP <sub>i</sub> buffer (pH 9.2, $n = 10 \text{ mV} \cdot \text{s}^{-1}$ ) demonstrating the enhanced catalytic currents associated with <b>2</b> .....	43
<b>Figure 3-7.</b> Catalytic Cycle of $[Ru^{II}(\text{Mebimpy})(4,4'\text{-bis-methylenephosphonato-2,2'-bipyridine})(OH_2)]^{2+}$ .....	44

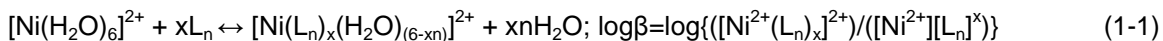
## Chapter 1: Introduction

### 1-1 Introduction of coordination chemistry and pentadentate ligands:

Modern coordination chemistry began with Alfred Werner's work concerning the spatial arrangement of atoms in molecules. Soon after finishing his dissertation in 1893, he authored a paper that described his theory of variable valence for inorganic materials. He claimed that the most common coordination numbers were three, four, six, and eight and concluded that six occurred the most often. This work, along with hundreds of other papers over the next 20 years, contributed to his receipt of the 1913 Nobel Prize for Chemistry.<sup>1</sup> Some of Werner's work dealt with dinuclear cobalt complexes that reacted with oxygen to form an O-O bridging ligand. Elemental analysis and reactivity were initially the primary methods used to characterize such complexes. X-ray diffraction, vibrational, and EPR spectroscopy were later implemented to discern the identity of the O-O bridging ligand as either superoxo ( $\text{O}_2^-$ ) or peroxo ( $\text{O}_2^{2-}$ ).<sup>2</sup> Modern crystallographic methods are now used in many classes of complexes to identify a range of bond distances characteristic of a pair of ions in each class. For example, for a superoxide ion that bridges two Co(III) centers, the O-O bond distance ranges from 1.26 to 1.36 Å.<sup>3</sup> Such information can be used to predict bond distances in new complexes of this kind. Many mononuclear cobalt(II) complexes were later found that reacted with gaseous  $\text{O}_2$  in aqueous solutions in order to make  $\mu$ -peroxo species. These complexes could be oxidized further with hydrogen peroxide to make  $\mu$ -superoxo complexes.<sup>4</sup> Further research in the oxygen binding capabilities of other simple cobalt complexes has continued over the years.

With the growth of X-ray diffraction capabilities throughout the 1960's,<sup>5</sup> it was found that certain ligand coordination environments are more prevalent than others in biological systems. Species with  $\text{MN}_5\text{X}$  or  $\text{MN}_4\text{XY}$  coordination environments were found in many metalloproteins. Prevalent examples include the iron-containing heme unit in (oxy)hemoglobin<sup>6</sup> and myoglobin,<sup>7</sup> the cobalt-containing corrin unit in vitamin B12,<sup>8</sup> and magnesium-centered chlorophyll molecules in Photosystem II.<sup>9</sup>

Multidentate ligands are comprised of organic scaffolds with more than one Lewis donor site that can bind a metal center. Interest in these ligands has arisen due to the high stability they impart to metal complexes compared to complexes with independent Lewis bases. This trend can be illustrated by comparing stability constants between various nickel(II) complexes with some common ligands. (See Equation 1-1 and Table 1-1.)<sup>10,11</sup>



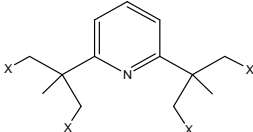
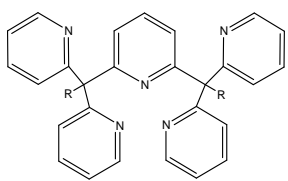
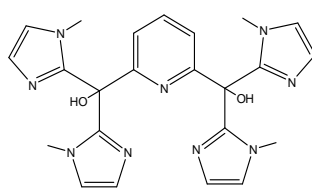
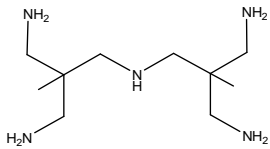
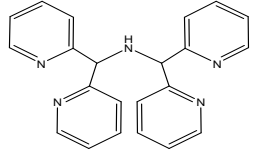
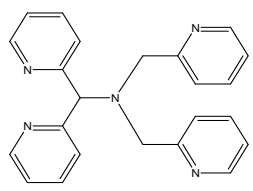
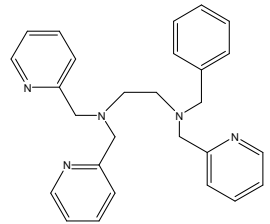
Ligand (L)	Structure	x	n	Log $\beta$
NH <sub>3</sub>		2	1	5.0
		4	1	7.9
		6	1	8.6
en		1	2	7.5
		2	2	13.9
		3	2	18.3
dien		1	3	11.0
trien		1	4	14.4
tetren		1	5	17.4
penten		1	6	19.1

**Table 1-1:** Stability constants for various nickel (II) complexes. (n=denticity of ligand, x=number of ligands). Reproduced from references 10 and 11.

The data indicates that the hexadentate complex  $[\text{Ni}(\text{penten})]^{2+}$  is more stable than the hexaammine complex  $[\text{Ni}(\text{NH}_3)_6]^{2+}$  by about 10 orders of magnitude. This extra stability is mostly entropic in nature, as the donor abilities of ammonia and other amines toward  $\text{Ni}^{2+}$  do not differ significantly. It is also well-known that the stability constants and even the reactivity of complexes with polydentate ligands depend on the types of groups and relative  $\text{pK}_a$ 's of donors binding to a given metal.<sup>12</sup> Therefore, the chemistry observed for one multidentate ligand may not be the same as that for another of similar structure.

### **1-2 Pentadentate Ligands that Support Transition Metal Complexes:**

Of the various multidentate ligands, pentadentate N5 ligands have proven to be exceptionally useful for studying various reactions. When coordinated to transition metal centers, pentadentate ligands provide stability to the complex and a weakly-bound exogenous ligand can provide a binding site for the substrate. Grohmann has developed a useful classification scheme for pentadentate AE4-type (A = axial, E = equatorial) tetrapodal ("four-legged") ligands that subdivides these species into four different types, as summarized in Table 1-2. Class I ligands have a 2,6-disubstituted pyridine unit at the axial site and aliphatic sidearms. Class II ligands have a heteroaromatic ring at the axial site and aromatic sidearms. Class III ligands have a non-aromatic donor group at the axial site. Class IV ligands are tetrapodal but have a lower point group than  $\text{C}_{2v}$ .<sup>13</sup>

Class I:		X=NH <sub>2</sub> , OH, PR <sub>2</sub>
Class II:		R=H; PY5-H R=Me; PY5-Me R=OH; PY5-OH R=OMe; PY5
		Im4PY
Class III:		ditame
		PY4N
Class IV:		N4PY
		Bztpen

**Table 1-2:** Examples of four different classes of pentadentate ligands.<sup>13</sup>

There are many examples of pentadentate ligands that have been used in transition-metal catalysts. These catalysts have been used in water splitting, both as water reduction catalysts<sup>14,15</sup> and as water oxidation catalysts.<sup>16,17</sup> They have also been used in the activation of small molecules other than water, such as C-H activation.<sup>18-20</sup> The N4PY ligand has been used to

activate triplet-state dioxygen, which can be used in DNA cleavage.<sup>21</sup> Another interesting example of the reactivity of metal complexes of pentadentate ligands involves the reduction of copper(II) by nitric oxide to create an N-nitrosoamine.<sup>22</sup> Finally, there have been many biomimetic studies that use pentadentate ligands coordinated to single metal sites to study the mechanisms of reactions exhibited by some biological systems.<sup>23-26</sup>

### 1-3 Previously Studied pz<sub>4</sub>lut Transition Metal Complexes:

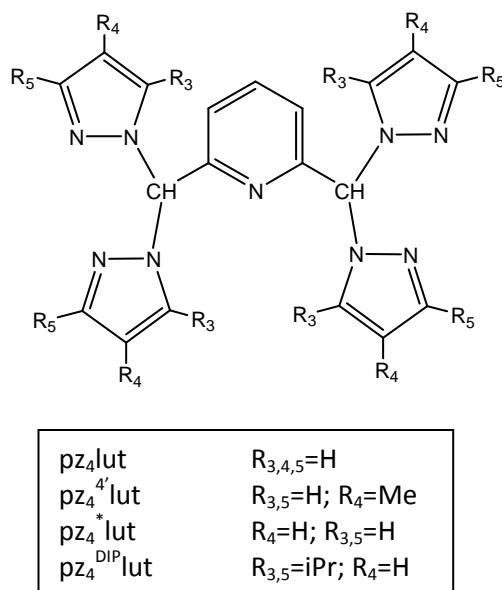


**Figure 1-1:** A new set of class II AE4 tetrapodal pentadentate ligands, pz<sup>R</sup><sub>4</sub>lut.

A new set of class II AE4 tetrapodal pentadentate ligands, pz<sup>R</sup><sub>4</sub>lut, that have pyrazolyl side arms and a pyridyl anchor, was recently reported.<sup>27</sup> These ligands are relatives of the more intensely-studied PY5-R class of ligands. (See Figure 1-1.) The pz<sup>R</sup><sub>4</sub>lut ligands were prepared by the CoCl<sub>2</sub>-catalyzed rearrangement of 2,6-pyridinedicarboxaldehyde and S(O)(pz<sup>R</sup>)<sub>2</sub>. The structures and electronic absorption spectra of first-row transition metal complexes of the parent ligand, pz<sub>4</sub>lut, were studied to ascertain the best fit for the ligand binding pocket and how the electron donor properties of this new pentadentate ligand compared to PY5 derivatives. Examination of the various structural parameters about the metal and ligand framework showed that the ligand fits best around the NiCl<sup>+</sup> moiety versus other MCl<sup>+</sup> units (M=Mn-Zn). Three

derivatives of pz<sub>4</sub>lut were later synthesized to study the impact of alkyl substitution on the binding modes of silver(I) complexes.<sup>28</sup> Also, a comparison of electronic spectrum of [CoLCl]<sup>+</sup> species (L = pz<sub>4</sub>lut and PY5) demonstrated that the pz<sub>4</sub>lut ligand was a slightly better donor than PY5. This result was slightly surprising since pyridyls are generally stronger-field donors than pyrazolyl groups. This apparent discrepancy was attributed to the greater steric issues of organizing three six-membered rings and a methoxy group (in PY5) versus three five-membered rings and a hydrogen atom (in pz<sub>4</sub>lut) about a central carbon, which cause greater ligand distortions and less overlap of metal and ligand orbitals.

One focus of this thesis was to test the hypothesis that steric issues can give rise to the discrepancy in the expected order of ligand field strengths of pentadentate ligands. The substitution along the pz<sub>4</sub><sup>R</sup>lut periphery was systematically varied to examine the influence on the electronic properties of the resultant complexes. Such information can also be used to uncover new chemical reactivity. Toward this first goal, Chapter 2 describes new chemical reactions that can be used to modify the pz<sub>4</sub>lut backbone. The influence of such substitution patterns on the electronic properties of iron(II) chloride complexes was studied. As some of these complexes show significant changes in structure upon cooling from room temperature, there may be a spin-state change from high spin to low spin. The corresponding cobalt complexes were also prepared to see if there is an analogous spin transition. Chapter 3 continues with the comparison of PY5 versus pz<sub>4</sub>lut-type complexes via examination of the potential proton-coupled electron transfer (PCET) events and water oxidation capabilities of aquacobalt complexes. The thesis concludes with a summary and outlook for further research.

## Chapter 2: Iron(II) Chloride Complexes of $\text{pz}^{\text{R}}_4\text{lut}$ and $\text{pz}^{\text{R}}_4\text{depy}$

### 2-1 Introduction:

The frequent occurrence of the  $\text{FeN}_5\text{X}$  coordination sphere in biological systems has served as an inspiration for the design of man-made iron complexes with nitrogenous pentadentate ligands.<sup>1</sup> Studies of the coordination chemistry of such model systems have significantly improved our understanding of natural metalloenzymes and led to important new chemical discoveries in research areas ranging from bioinorganic to materials chemistry. An outstanding group of these pentadentate ligand systems is the PY5-R class (see Chapter 1).

Iron PY5-R complexes have been employed in a variety of biological and non-biological inorganic studies. For instance, like several lipoxygenase non-heme iron enzymes,  $[\text{Fe}(\text{OMe})(\text{PY5})](\text{OTf})_2$  is capable of C-H activation.<sup>2</sup> Metastable low spin  $[\text{Fe}(\text{OOH})(\text{PY5})](\text{ClO}_4)_2$  could be trapped and studied spectroscopically, providing insight into intermediates implicated in oxygen-activating biomolecules.<sup>3</sup> Recently,  $[\text{Fe}(\text{CH}_3\text{CN})(\text{PY5-OH})](\text{ClO}_4)_2$  was reported to be a more potent anti-tumor agent than cis-platin.<sup>4</sup> Also, fundamental systematic studies of  $[\text{Fe}^{\text{II}}(\text{X})(\text{PY5})]^{n+}$  complexes involving variation of the exogeneous ligand X led to the discovery of two complexes, where X is  $\text{N}^{3-}$  or MeOH, that exhibit spin-state changes.<sup>5</sup> The latter complex,  $[\text{Fe}^{\text{II}}(\text{MeOH})(\text{PY5})](\text{OTf})_2$ , represents a rare example of a spin-crossover complex with an  $\text{Fe}^{\text{II}}\text{N}_5\text{O}$  donor set; most such examples contain a  $\text{Fe}^{\text{II}}\text{N}_6$  coordination environment.<sup>6</sup> Such discoveries may have important implications in future ligand designs for the development of spin-crossover materials for memory devices<sup>7</sup> and optical devices.<sup>8</sup>

Recently, a set of tetra(pyrazolyl)lutidines,  $\text{pz}^{\text{R}}_4\text{lut}$ , was studied. This set of ligands are related to PY5-R.<sup>9</sup> The ready availability of the nearly endless pyrazole variants and the simple synthetic routes to the  $\text{pz}^{\text{R}}_4\text{lut}$  ligands presage numerous avenues for study in coordination chemistry. Initial investigations focused on examining what impact, if any, that substitution of hydrogens for methyl groups along the ligand periphery has on the electronic properties of iron(II) chloride complexes.<sup>10</sup> Herein is described some rather attractive results concerning the influence



of substitution patterns on the properties of the iron(II) complexes. A new addition to the  $\text{pz}^{\text{R}}_4\text{lut}$  family of ligands is introduced, and a simple reaction sequence that can be used to modify the ligand backbone at the methine carbon atoms is described.

## 2-2 Synthesis:

**General Considerations.** MeI, n-BuLi, and  $\text{FeCl}_2$  were purchased from commercial sources and used as received. Literature procedures were used for the preparations of  $\text{pz}^*_4\text{lut}$ ,  $\text{pz}^{4\text{Me}}_4\text{lut}$ ,<sup>9</sup>  $\text{pz}_4\text{lut}$ , **1**•2MeOH, **3**•2MeOH, and **4**•1.75MeOH.<sup>10</sup> Solvents were dried by conventional methods and distilled prior to use. All syntheses were carried out under a nitrogen atmosphere by using standard Schlenk techniques.

Midwest MicroLab, LLC in Indianapolis, Indiana performed all elemental analyses.  $^1\text{H}$  and  $^{13}\text{C}$  NMR spectra were recorded on a Varian 400 MHz spectrometer. Chemical shifts were referenced to solvent resonances at  $\delta_{\text{H}}$  7.26 and  $\delta_{\text{C}}$  77.23 for  $\text{CDCl}_3$ ,  $\delta_{\text{H}}$  1.96 and  $\delta_{\text{C}}$  118.9 for  $\text{CD}_3\text{CN}$ . Absorption measurements were recorded on an Agilent 8453 spectrometer. Melting point determinations were made on samples contained in glass capillaries using an Electrothermal 9100 apparatus and are uncorrected. Solid state magnetic susceptibility measurements were performed using a Johnson-Matthey MSB-MK1 instrument. The magnetic moments were also measured in MeOH solution by the Evan's method.<sup>11</sup> Electrochemical measurements were collected under a nitrogen atmosphere at a scan rate of 100 mV/s for samples that were ~1 mM  $\text{CH}_3\text{OH}$  solutions with 0.1 M  $\text{NBu}_4\text{HSO}_4$  as the supporting electrolyte. A three-electrode cell comprised of an Ag/AgCl electrode (separated from the reaction medium with a semipermeable polymer membrane filter), a platinum working electrode, and a glassy carbon counter electrode was used for the voltammetric measurements. In this cell, the ferrocene/ferrocenium couple had an  $E_{1/2}$  value of +0.47 V.<sup>12</sup> X-ray powder diffraction measurements were performed with a Rigaku MiniFlex II instrument by using Cu K $\alpha$  (1.54178 Å) radiation.

**General procedure for methylating  $\text{pz}_4^{\text{R}}\text{lut}$  at methine positions.** To a cold (-78 °C), stirred solution of  $\text{pz}_4^{\text{R}}\text{lut}$  (1 equiv.) in THF was slowly added n-BuLi (1.6 M in hexanes, 2 equiv.)

to make a reddish solution. After 45 minutes, MeI (4 equiv.) was added. The reaction mixture was left to stir and warm to room temperature for 30 minutes, and water was added to quench the reaction. Then, 50 mL of CH<sub>2</sub>Cl<sub>2</sub> were added, and the mixture was carefully swirled. The aqueous layer was washed twice with two 50-mL portions of CH<sub>2</sub>Cl<sub>2</sub>, and the combined organics were dried over MgSO<sub>4</sub> and concentrated via rotary evaporation.

**pz<sub>4</sub><sup>4Me</sup>depy.** The reaction between 1.176 g (2.75 mmol) of pz<sub>4</sub><sup>4Me</sup>lut, 3.44 mL (5.50 mmol) of n-BuLi, and 0.68 mL (1.55 g, 10.9 mmol) of MeI in 20 mL of THF afforded 0.868 g (69%) of pz<sub>4</sub><sup>4Me</sup>depy as a colorless solid after purification by column chromatography on silica with Et<sub>2</sub>O as the eluent (R<sub>f</sub> 0.60 on a silica plate). Mp, 113-116°C. Anal. Calcd. (obsd.) for C<sub>25</sub>H<sub>29</sub>N<sub>9</sub>: C, 65.91 (65.88); H, 6.42 (6.37); N, 27.67 (27.21). <sup>1</sup>H NMR (CDCl<sub>3</sub>): δ 7.61 (t, J = 8 Hz, 1H, H<sub>4</sub>-py), 7.41 (s, 4H, H<sub>3</sub>-pz), 6.85 (s, 4H, H<sub>5</sub>-pz), 6.39 (d, J = 8 Hz, 2H, H<sub>3,5</sub>-py), 2.59 (s, 6H, CH<sub>3</sub>), 2.03 (s, 12H, CH<sub>3</sub>). <sup>13</sup>C NMR (CDCl<sub>3</sub>): δ 159.3, 140.9, 138.4, 128.3, 121.0, 116.5, 82.3, 26.3, 9.0. UV-Vis (CH<sub>3</sub>CN) λ<sub>max</sub>, nm (ε, M<sup>1</sup>cm<sup>-1</sup>): 226 (22,600), 262 (6,500).

**pz<sub>4</sub>depy.** The reaction between 1.50 g (4.04 mmol) of pz<sub>4</sub>lut, 5.05 mL (8.08 mmol) of n-BuLi, and 1.7 mL (27.3 mmol) of MeI in 40 mL of THF afforded 1.24 g (77%) of pz<sub>4</sub>depy as a fluffy, colorless solid after aqueous workup and column chromatography on silica with Et<sub>2</sub>O as the eluent (R<sub>f</sub>=0.55 on a silica plate). Mp, 157-159°C. Anal. Calcd. (obsd.) for C<sub>21</sub>H<sub>21</sub>N<sub>9</sub>: C, 63.14 (63.17); H, 5.30 (5.10); N, 31.56 (31.50). <sup>1</sup>H NMR (CDCl<sub>3</sub>): δ 7.65 (t, J = 7.8 Hz, 1H, H<sub>4</sub>-py), 7.61 (d, J = 2Hz, 4H, H<sub>3</sub>-pz), 7.13 (d, J = 1 Hz, 4H, H<sub>5</sub>-pz), 6.45 (d, J = 7.8 Hz, 2H, H<sub>3,5</sub>-py), 6.27 (dd, J = 1; 2Hz, 4H, H<sub>4</sub>-pz), 2.65 (s, 6H, CH<sub>3</sub>). <sup>13</sup>C NMR (CDCl<sub>3</sub>): δ 159.1, 140.3, 138.5, 129.6, 121.1, 106.1, 82.5, 26.4. UV-Vis (CH<sub>3</sub>CN) λ<sub>max</sub>, nm (ε, M<sup>1</sup>cm<sup>-1</sup>): 212 (35,000), 263 (6,500).

**[Fe(Cl)(pz<sub>4</sub>lut)]Cl·2MeOH, 1·2MeOH.** See Reference 10 For synthetic details.

**[Fe(Cl)(pz<sub>4</sub><sup>4Me</sup>lut)]Cl·2MeOH, 2·2MeOH.** Similar to the procedure above, a mixture of 0.290 g (0.678 mmol) pz<sub>4</sub><sup>4Me</sup>lut and 0.086 g (0.68 mmol) FeCl<sub>2</sub> in 20 mL CH<sub>3</sub>OH gave a total yield, 0.270 g, 66 % (0.260 g insoluble portion and 0.010 g from filtrate) of 2·2MeOH as an orange microcrystalline powder. Mp, 250 °C (decomp.). Anal. Calcd. (obsd.) for C<sub>25</sub>H<sub>33</sub>N<sub>9</sub>Cl<sub>2</sub>FeO<sub>2</sub>: C, 48.56 (48.88); H, 5.38 (5.75); N, 20.39 (20.51). μ<sub>eff</sub> (solid, 297 K): 5.6 ± 0.2 μ<sub>B</sub>. μ<sub>eff</sub> (Evans, CD<sub>3</sub>OD): 5.2 ± 0.1 μ<sub>B</sub>. UV-Vis (CH<sub>3</sub>OH) λ<sub>max</sub>, nm (ε, M<sup>1</sup>cm<sup>-1</sup>): 216 (18,400), 271 (3,900), 300

(1200), 462 (200), 874 (5), 960 (4). Slow cooling a hot supersaturated MeOH solution over several hours to room temperature affords very small crystals **2**·2MeOH that were not suitable for single crystal X-ray diffraction. X-ray quality crystals of  $[\text{FeCl}(\text{pz}^{4\text{Me}}_4\text{lut})](\text{Cl})\cdot\text{MeOH}\cdot 0.35\text{Et}_2\text{O}$ , **2**·MeOH·0.35Et<sub>2</sub>O were obtained by slow evaporation of solvents from an unsuccessful attempt at crystallization by vapor diffusion of Et<sub>2</sub>O into MeOH solution of the complex. A crystalline sample exposed to the laboratory atmosphere over the course of about a week analyzed as the hydrate, **2**·H<sub>2</sub>O: Anal. Calcd (found) for C<sub>23</sub>H<sub>27</sub>N<sub>9</sub>Cl<sub>2</sub>FeO: C, 48.27 (48.05); H, 4.76 (4.47); N, 22.03 (21.71). A powdered sample exposed to the laboratory atmosphere over the course of two weeks analyzed as the dihydrate, **2**·2H<sub>2</sub>O: Anal. Calcd. (found) for C<sub>23</sub>H<sub>29</sub>N<sub>9</sub>Cl<sub>2</sub>FeO<sub>2</sub>: C, 46.80 (47.06); H, 4.95 (4.59); N, 21.36 (20.98).

**[Fe(Cl)(pz\*<sub>4</sub>lut)]Cl·2MeOH, 3·2MeOH.** See Reference 10 for synthetic details.

**[Fe(Cl)(pz\*\*<sub>4</sub>lut)]Cl·1.75MeOH, 4·1.75MeOH.** See Reference 10 for synthetic details.

**[Fe(Cl)(pz<sub>4</sub>depy)]Cl·MeOH, 5·MeOH.** In a procedure similar to the above, a mixture of 0.159 g (1.25 mmol) FeCl<sub>2</sub> and 0.500 g (1.25 mmol) pz<sub>4</sub>depy in 30 mL CH<sub>3</sub>OH gave a total yield of 0.633 g (91 %) (0.033 g insoluble and 0.600 g from filtrate) of **5**·MeOH as a dark red-orange powder. Mp, 235 – 242 °C (decomp.). Anal. Calcd. (obsd.) for C<sub>22</sub>H<sub>25</sub>N<sub>9</sub>Cl<sub>2</sub>FeO: C, 47.34 (46.98); H, 4.51 (4.67); N, 22.58 (22.18).  $\mu_{\text{eff}}$  (solid, 297 K):  $2.9 \pm 0.1 \mu_{\text{B}}$ .  $\mu_{\text{eff}}$  (Evans, MeOH 295 K):  $2.8 \pm 0.1 \mu_{\text{B}}$  (also see below). <sup>1</sup>H NMR (CD<sub>3</sub>OD, 273 K)  $\delta_{\text{H}}$  9.12 (br s, 4H), 8.93 (br s, 4H), 8.39 (br d,  $J = 8.1$  Hz, 2H), 8.15 (br t,  $J = 8.1$  Hz, 1 H), 7.07 (br s, 4H), 3.41 (br s, 6H). UV-Vis (CH<sub>3</sub>OH)  $\lambda_{\text{max}}$ , nm ( $\epsilon$ ,  $M^{-1}\text{cm}^{-1}$ ): 214 (31,000), 268 (10,500), 305 (7,600), 390 (2,300), 462 (3,000). X-ray quality crystals were obtained by vapor diffusion of Et<sub>2</sub>O into a MeOH solution of **5** or by slowly cooling a supersaturated solution (30-40 mg of **5** in 1 mL MeOH) from 60°C to room temperature over the period of 24 h.

**[FeClpz<sup>4Me</sup><sub>4</sub>depy]Cl·MeOH, 6·MeOH.** In a procedure similar to the above, a mixture of 0.0765 g (0.603 mmol) of FeCl<sub>2</sub> and 0.532 g (0.603 mmol) of pz<sup>4Me</sup><sub>4</sub>depy in 30 mL of methanol, gave a total yield of 0.304 g (82%) of **6**·MeOH as a rose-red powder. Mp, orange at 170 °C, 223-230 °C (decomp., red-black liquid). Anal. Calcd. (obsd.) for C<sub>26</sub>H<sub>33</sub>N<sub>9</sub>Cl<sub>2</sub>FeO: C, 50.83 (50.45); H, 5.41 (5.60); N, 20.52 (20.16).  $\mu_{\text{eff}}$  (solid, 297 K):  $3.4 \pm 0.1 \mu_{\text{B}}$ .  $\mu_{\text{eff}}$  (Evans, MeOH, 295 K):  $2.0 \pm$

0.1  $\mu_B$ .  $^1\text{H}$  NMR ( $\text{CD}_3\text{OD}$ , 293 K)  $\delta_{\text{H}}$  8.95 (br s, 4H), 8.67 (br s, 4H), 8.39 (br s, 2H), 7.98 (br s, 1H), 3.15 (br s, 6H), 2.24 (s, 12H,  $\text{CH}_3$ ). UV-vis ( $\text{CH}_3\text{OH}$ )  $\lambda_{\text{max}}$ , nm ( $\epsilon$ ,  $M^{-1}\text{cm}^{-1}$ ): 215 (22,000), 272 (7,500), 308 (7,200), 400 (1,200), 468 (3,100). Good, but not X-ray quality, small needle crystals were obtained by vapor diffusion of  $\text{Et}_2\text{O}$  into a  $\text{MeOH}$  solution of **6**. A sample left exposed to laboratory atmosphere for several days analyzed as a mixed solvate **6**• $\text{MeOH}$ • $\text{H}_2\text{O}$ . Anal. Calcd. (obsd). for  $\text{C}_{26}\text{H}_{35}\text{N}_9\text{Cl}_2\text{FeO}_3$ : C, 47.19 (47.28); H, 5.54 (4.95); N 19.81 (19.68).

**[Co(Cl)(pz<sub>4</sub>depy)]Cl•MeOH, 7•MeOH**. In a procedure similar to the above, a mixture of 0.159 g (1.25 mmol)  $\text{CoCl}_2$  and 0.500 g (1.25 mmol)  $\text{pz}_4\text{depy}$  in 30 mL  $\text{CH}_3\text{OH}$  gave a total yield of 0.633 g (91%) (0.033 g insoluble and 0.600 g from filtrate) of **7**• $\text{MeOH}$  as a dark red-orange powder. Mp: 235—242 °C (decomp.). Anal. Calcd. (obsd.) for  $\text{C}_{22}\text{H}_{25}\text{N}_9\text{Cl}_2\text{FeO}$ : C, 47.34 (46.98); H, 4.51 (4.67); N, 22.58 (22.18).  $\mu_{\text{eff}}$  (solid, 297 K):  $2.9 \pm 0.1 \mu_B$ .  $\mu_{\text{eff}}$  (Evans, 297 K):  $2.9 \pm 0.1 \mu_B$

### 2-3 Crystallography:

Crystal structures of **1**• $\text{MeOH}$ , **1**•2 $\text{MeOH}$ , **2**• $\text{MeOH}$ •0.35 $\text{Et}_2\text{O}$ , **3**• $\text{MeOH}$ , **3**•2 $\text{MeOH}$ , **4**•1.75 $\text{MeOH}$  have been reported previously.<sup>10</sup> A red-brown prism of  $[\text{FeCl}(\text{pz}_4\text{depy})]\text{Cl}$ • $\text{MeOH}$ , **5**• $\text{MeOH}$ , was collected at 100(2) K with an Oxford Diffraction Ltd. Supernova equipped with a 135 mm Atlas CCD detector, by using  $\text{Mo K}\alpha$  radiation,  $\lambda = 0.7107 \text{ \AA}$ . A second red-brown block of **5**• $\text{MeOH}$  was used for a room temperature (296(2) K) diffraction experiment using the latter instrument with  $\text{Cu K}\alpha$  radiation,  $\lambda = 1.54178$ . Raw data frame integration and Lp corrections were performed with SAINT+<sup>13</sup> for the data collected from the Bruker instrument but with CrysAlisPro<sup>14</sup> for that from the Oxford instrument. Final unit cell parameters were determined by least-squares refinement of 15602 and 4265 reflections from the 100 K and 296 K experiments, respectively, of **5**• $\text{MeOH}$ , with  $I > 2\sigma(I)$ . Analysis of the data showed negligible crystal decay during collection in each case. Direct methods structure solutions, difference Fourier calculations and full-matrix least-squares refinements against  $F^2$  were performed with SHELXTL.<sup>15</sup> All non-hydrogen atoms were refined with anisotropic displacement parameters. Hydrogen atoms were placed in geometrically idealized positions and included as riding atoms. The X-ray

crystallographic parameters and further details of data collection and structure refinements are presented in Tables 2-1 and 2-2.

Compound	5•MeOH	5•MeOH
Formula	C <sub>22</sub> H <sub>25</sub> Cl <sub>2</sub> FeN <sub>9</sub> O	C <sub>22</sub> H <sub>25</sub> Cl <sub>2</sub> FeN <sub>9</sub> O
Formula weight	558.26	558.26
Crystal system	Monoclinic	Monoclinic
Space group	C 2/c	C 2/c
Temp. [K]	100(2)	296(2)
<i>a</i> [Å]	23.7571(8)	24.0175(7)
<i>b</i> [Å]	11.5527(2)	11.6568(3)
<i>c</i> [Å]	19.0958(7)	19.2632(6)
$\alpha$ [°]	90	90
$\beta$ [°]	116.246(4)	116.234(4)
$\gamma$ [°]	90	90
<i>V</i> [Å <sup>3</sup> ]	4700.7(3)	4837.6(2)
<i>Z</i>	8	8
<i>D</i> <sub>calcd.</sub> [gcm <sup>-3</sup> ]	1.578	1.533
$\lambda$ [Å] (Mo K $\alpha$ )	0.7107	1.54178
$\mu$ [mm <sup>-1</sup> ]	0.906	7.332
Abs. Correction	multi-scan	numerical
<i>F</i> (000)	2304	2304
$\theta$ range [°]	3.31 to 29.42	4.10 to 73.82
Reflections collected	27409	10206
Independent reflections	6015 ( <i>R</i> <sub>int</sub> 0.0231)	4752 ( <i>R</i> <sub>int</sub> 0.0236)
<i>T</i> <sub>min</sub> /max	0.90513/1.0	0.293/0.516
Data/restraints/ parameters	6015/0/320	4752/0/324
Goodness-of-fit on <i>F</i>	1.059	1.041
<i>R</i> 1/ <i>wR</i> 2[ <i>I</i> > 2 $\sigma$ ( <i>I</i> )] <sup>a</sup>	0.0281/0.0725	0.0375/0.0935
<i>R</i> 1/ <i>wR</i> 2 (all data) <sup>a</sup>	0.0350/0.0745	0.0433/0.0986
Largest diff. peak/hole(□/□ e Å <sup>-3</sup> )	0.450/-0.384	0.750/-0.762
<sup>a</sup> $R1 = \sum   F_o  -  F_c   / \sum  F_o $ $wR2 = [\sum w( F_o  -  F_c )^2 / \sum w F_o ^2]^{1/2}$ .		

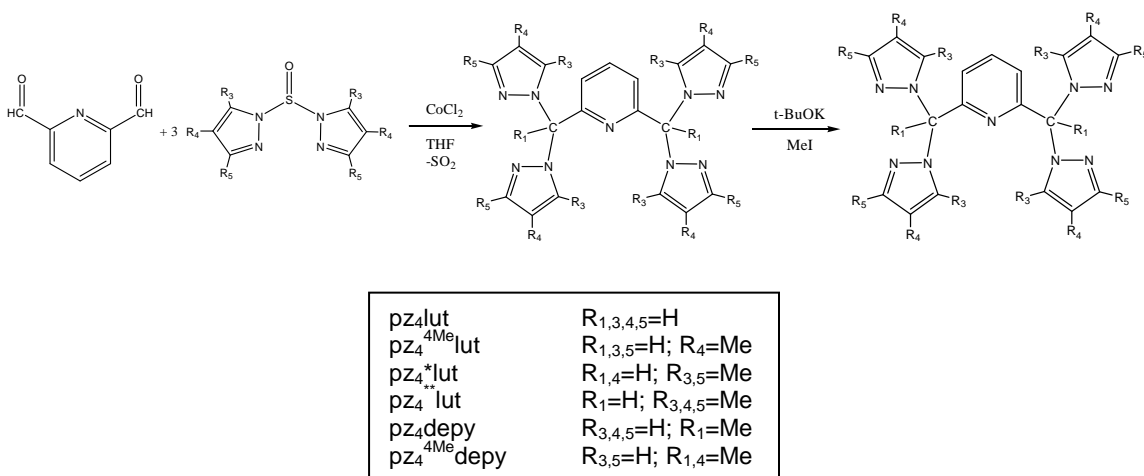
**Table 2-1.** Crystallographic data for 5•MeOH at T=100 K and 296 K.

Compound	7·MeOH	7·MeOH
Formula	C <sub>22</sub> H <sub>25</sub> Cl <sub>2</sub> CoN <sub>9</sub> O	C <sub>22</sub> H <sub>25</sub> Cl <sub>2</sub> CoN <sub>9</sub> O
Formula weight	561.34	561.34
Crystal system	monoclinic	monoclinic
Space group	C 2/c	C 2/c
Temp. [K]	296(2)	100(2)
<i>a</i> [Å]	24.1290(11)	23.8606(8)
<i>b</i> [Å]	11.7105(3)	11.6501(3)
<i>c</i> [Å]	19.3867(8)	19.2923(7)
$\alpha$ [°]	90	90
$\beta$ [°]	116.285(6)	116.198(4)
$\gamma$ [°]	90	90
<i>V</i> [Å <sup>3</sup> ]	4911.6(3)	4811.9(3)
<i>Z</i>	8	8
<i>D</i> <sub>calcd.</sub> [gcm <sup>-3</sup> ]	1.518	1.550
$\lambda$ [Å] (Mo K $\alpha$ )	0.7107	0.7107
$\mu$ [mm <sup>-1</sup> ]	0.952	0.972
Abs. Correction	multi-scan	multi-scan
<i>F</i> (000)	2312	2312
$\theta$ range [°]	3.32 to 29.60	3.39 to 29.54
Reflections collected	28414	27942
Independent reflections	6308 ( <i>R</i> <sub>int</sub> 0.0248)	6146 ( <i>R</i> <sub>int</sub> 0.0265)
<i>T</i> <sub>min</sub> /max	0.86035/1.00000	0.86692/1.00000
Data/restraints/ parameters	6308/0/323	6146/0/323
Goodness-of-fit on <i>F</i> <sup>2</sup>	1.0056	1.040
<i>R</i> 1/ <i>wR</i> 2 [ <i>I</i> > 2 $\sigma$ ( <i>I</i> )] <sup>a</sup>	0.0334/0.0761	0.0293/0.0637
<i>R</i> 1/ <i>wR</i> 2 (all data) <sup>a</sup>	0.0485/0.0851	0.0374/0.0682
Largest diff. peak/hole/e Å <sup>-3</sup>	0.476/-0.419	0.391/-0.335
<sup>a</sup> <i>R</i> 1 = $\sum   F_o  -  F_c   / \sum  F_o $ <i>wR</i> 2 = $[\sum w( F_o  -  F_c )^2 / \sum w F_o ^2]^{1/2}$ .		

**Table 2-2.** Crystallographic data collection and structure refinement for [CoCl(pz<sub>4</sub>depy)]Cl·MeOH, 7·MeOH at T=296 K and T=100 K.

## 2-4 Results:

**Syntheses.** As outlined in the second part of Scheme 2-1, the new ligands in this work,  $\text{pz}^{\text{R}}_4\text{depy}$ , were prepared by an extension of the derivatization chemistry known for tris(pyrazolyl)methane ligands.<sup>16</sup> That is, alkylation of  $\text{pz}^{\text{R}}_4\text{lut}$  at the methine carbons was achieved by the reaction between the ligand and a deprotonating agent followed by addition of excess iodomethane as an electrophile.



**Scheme 2-1.** Preparation of  $\text{pz}^{\text{R}}_4\text{lut}$  ligands described in this work.

The reactions between methanol solutions of anhydrous  $\text{FeCl}_2$  and the various  $\text{pz}^{\text{R}}_4\text{lut}$  ligands resulted in the precipitation of microcrystalline powders of the iron(II) complexes  $[\text{FeCl}(\text{pz}_4\text{lut})]\text{Cl}\cdot 2\text{MeOH}$  (**1**·2MeOH),  $[\text{FeCl}(\text{pz}_4^{4\text{Me}}\text{lut})]\text{Cl}\cdot \text{MeOH}$  (**2**·MeOH),  $[\text{FeCl}(\text{pz}_4^{*\text{lut}})]\text{Cl}\cdot 2\text{MeOH}$  (**3**·2MeOH), and  $[\text{FeCl}(\text{pz}_4^{**}\text{lut})]\text{Cl}\cdot 2\text{MeOH}$  (**4**·2MeOH),  $[\text{FeCl}(\text{pz}_4\text{depy})]\text{Cl}\cdot \text{MeOH}$  (**5**·MeOH), and  $[\text{FeCl}(\text{pz}_4^{4\text{Me}}\text{depy})]\text{Cl}\cdot \text{MeOH}$  (**6**·MeOH) in high yield. The complexes exhibit relatively low solubilities in methanol of ca. 0.004, 0.01, 0.02, and 0.03 M for **1-4**, respectively, and are practically insoluble in most other organic solvents and in water. Complexes **1-4** are hygroscopic and form trihydrates,  $[\text{Fe}(\text{Cl})(\text{pz}^{\text{R}}_4\text{lut})](\text{Cl})\cdot 3\text{H}_2\text{O}$  (combustion analyses), when left unprotected under ambient conditions for a few weeks. For this reason, electrochemical and spectroscopic measurements were made on samples freshly crystallized from methanol and vacuum dried.

The reactions between  $\text{pz}^{\text{R}}_4\text{depy}$  and  $\text{FeCl}_2$  in methanol result in the immediate formation of  $[\text{FeCl}(\text{pz}^{\text{R}}_4\text{depy})](\text{Cl})$  ( $\text{R} = \text{H}$ , **5**; or  $\text{R} = 4\text{Me}$ , **6**) as indicated spectroscopically (vide infra) and visually by the color change from nearly colorless or pale yellow of the starting materials to deep red-orange. Complexes **5** and **6** are noticeably more soluble in methanol at ca. 0.04 and 0.2 M, respectively, than are **1-4**, and they do not precipitate to the extent of the other complexes depending on the concentration range of the preparative reaction. Room temperature magnetic susceptibility measurements indicate that complexes **1-6** are paramagnetic both in solution and in the solid state, vide infra. The 297 K solid-state values  $\mu_{\text{eff}} > 5 \mu_{\text{B}}$  for complexes **1-4** are typical for high-spin iron(II) with unquenched orbital angular momentum. In contrast, at 297 K, solid-state values of  $\mu_{\text{eff}} = 1.9\text{-}3.4 \mu_{\text{B}}$  were obtained for various samples of solid **5** or **6**. The magnetic data together with the solid-state thermochromic behavior of **5** and **6** which reveals that samples gradually change from red-orange (**5**) or rose-red (**6**) at room temperature to pale orange at ca. 180°C, are suggestive of spin-crossover behavior (vide infra). Complexes **1** and **2** are also noticeably thermochromic in the solid state but in the opposite sense—at low temperature (-196°C) the complexes are pale yellow and gradually become more orange upon warming to room temperature and above. Comparisons of high and low temperature single crystal X-ray diffraction data for **1**·CH<sub>2</sub>Cl<sub>2</sub> and **4**·1.75MeOH show comparable but insignificant variation in bond distances with temperature. Therefore, the solid-state thermochromic behavior of **1** and **2** is attributed to changes in the intensity and possibly the energy of charge-transfer electronic transitions (vide infra) rather than to changes in the electronic spin state of the iron(II).

**Solid State Structures.** Single crystals suitable for X-ray diffraction have been obtained for each  $[\text{FeCl}(\text{pz}^{\text{R}}_4\text{lut})](\text{Cl})$  complex and for  $[\text{FeCl}(\text{pz}_4\text{depy})](\text{Cl})\cdot\text{MeOH}$ , either by cooling hot supersaturated methanol solutions of **1-5** to give **1**·2MeOH, **3**·2MeOH, **4**·1.75MeOH, and **5**·MeOH or by diffusion of co-solvents into methanol solutions of **2** or **5** to give **2**·MeOH·0.35Et<sub>2</sub>O and **5**·MeOH. Suitable crystals of **6**·MeOH have not yet been obtained. Selected views of the structures of various  $[\text{FeCl}(\text{pz}^{\text{R}}_4\text{lut})]^+$  and  $[\text{FeCl}(\text{pz}_4\text{depy})]^+$  cations are found in Figures 2-1 through 2-4. Figure 2-3 shows the  $[\text{CoCl}(\text{pz}_4\text{depy})]^+$  cation. Selected bond distances and angles for the various complexes are given in Table 2-3. The ligand in each complex is pentadentate



and gives rise to a  $\text{FeN}_5\text{Cl}$  coordination environment. The iron-ligand bond distances in **1-4** are indicative of high-spin iron(II). For instance, the average  $\text{Fe-N}(\text{pyrazolyl})$ ,  $\text{Fe-N}_{\text{pz}}$ , bond distances in the complexes **1-4** are greater than  $2.10 \text{ \AA}$  (Table 2-4), values distinctive for high-spin iron(II) in a wide range of iron(II) complexes with pyrazolyl-containing ligands; low-spin iron(II) derivatives have average  $\text{Fe-N}_{\text{pz}}$  bond distances of ca.  $1.98 \text{ \AA}$ .<sup>17</sup> Similarly, the  $\text{Fe-N}(\text{pyridyl})$ ,  $\text{Fe-N}_{\text{py}}$ , bond distances in **1-4** ( $> 2.2 \text{ \AA}$ ) are typical of HS Fe(II) exemplified by the related PY5 complexes.<sup>18</sup> The  $\text{Fe-Cl}$  bond distance is rather insensitive to the ligand variation across the series **1-4** and remains in the narrow range of  $2.32$  to  $2.34 \text{ \AA}$ .

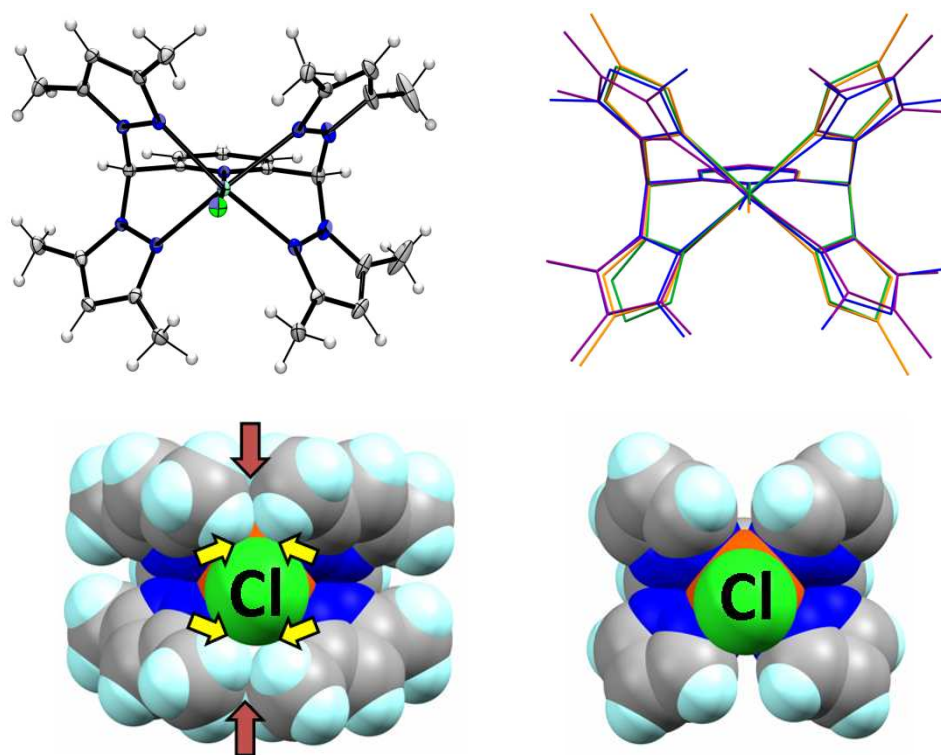


**Figure 2-1.** Top left: Structure of the cation in  $[\text{FeCl}(\text{pz}^*_4\text{lut})]\text{Cl}$  (**3**) shown with thermal ellipsoids at the 50% probability level; Top right: Overlay of all cation structures in **1** (green), **2** (orange), **3** (blue) and **4** (violet). Bottom: Space-filling representations for cations in **3** (left) and **1** (right) where the areas with potential steric interactions are highlighted by arrows.

Interestingly, inspection of the structures of the four complexes **1-4** (top right of Figure 2-1) and of the associated metric parameters in Table 2-4 reveals that these complexes can be divided into two subsets based on whether or not methyl groups occupy the 3-positions of the

pyrazolyls that are proximal to the iron-bound chloride. Complexes **3** and **4**, with 3-methyl substituents, each have longer average Fe-N<sub>pz</sub> bonds of 2.28 Å and relatively large average FeN-NC<sub>methine</sub> torsion angles of 7° for **3** and 14° for **4**, values that are indicative of greater pyrazolyl ring twisting, vide infra, as compared with the other two derivatives with hydrogen at the 3-position of the pyrazolyls (Fe-N<sub>pz</sub> 2.20 Å, FeN-NC<sub>methine</sub> 2° for **1** and Fe-N<sub>pz</sub> 2.18 Å, FeN-NC<sub>methine</sub> 5° for **2**). The space-filling models shown at the bottom of Figure 2-1 reveal that the dichotomy in the two types of structures may be due in part to two types of steric interactions: those between 3-methyl substituents, see the red arrows in Figure 2-1, and those interactions between 3-methyl pyrazolyl substituents and the axial chloride group see the yellow arrows in Figure 2-1. The increase in both the Fe-N<sub>pz</sub> bond lengths and in the twisting of the ligand pyrazolyl rings for **3** and **4** relative to **1** and **2** presumably alleviates unfavorable steric interactions in a similar, but less dramatic, manner than is found in related iron(II) tris(pyrazolyl)borate or tris(pyrazolyl)methane complexes where the spin states change depending on whether or not 3-methyl pyrazolyl substituents are present.<sup>17</sup>

Distances (Å)	1•MeOH	1•2MeOH	2•MeOH•0.35E	3•2MeO	4•1.75MeOH	5•MeOH 100	5•MeOH 296	
Fe1-Cl	2.3137(6)	2.3512(9)	2.3230(6)	2.3282(9)	2.3332(7)	2.3303(7)	2.3251(4)	2.3184(7)
Fe1-N1	2.243(1)	2.258(3)	2.268(2)	2.218(3)	2.207(2)	2.211(2)	1.932(1)	2.019(2)
Fe1-N11	2.188(1)	2.175(2)	2.169(2)	2.245(2)	2.322(2)	2.286(2)	1.960(1)	2.012(2)
Fe1-N21	2.188(1)	2.175(2)	2.185(2)	2.245(2)	2.307(2)	2.270(2)	1.969(1)	2.019(2)
Fe1-N31	2.205(1)	2.177(2)	2.182(2)	2.317(2)	2.261(2)	2.247(2)	1.958(1)	2.003(2)
Fe1-N41	2.205(1)	2.177(2)	2.175(2)	2.317(2)	2.257(2)	2.289(2)	1.956(1)	2.007(2)
Avg Axial	2.279(1)	2.305(2)	2.295(2)	2.273(2)	2.276(1)	2.271(1)	2.129(1)	2.169(1)
Avg Equatorial	2.197(1)	2.176(2)	2.177(2)	2.281(2)	2.287(2)	2.273(2)	1.961(1)	2.010(2)
Avg All	2.224(1)	2.219(2)	2.216(2)	2.278(2)	2.281(2)	2.272(2)	2.017(1)	2.063(2)
Angles (°)								
N1-Fe-Cl	176.29(4)	177.81(10)	177.98(5)	176.82(7)	178.91(5)	178.44(5)	178.14(4)	177.85(5)
N11-Fe1-N21	81.90(4)	82.14(7)	83.90(7)	82.81(9)	77.93(7)	78.22(7)	86.46(5)	85.63(8)
N31-Fe1-N41	81.90(4)	82.14(7)	83.99(7)	74.98(9)	79.76(7)	78.59(7)	87.55(5)	87.09(8)
N11-Fe1-N41	92.37(6)	96.63(13)	92.75(7)	99.18(6)	98.21(7)	101.45(7)	92.60(5)	92.82(7)
N21-Fe1-N31	98.56(6)	93.59(13)	92.89(7)	99.18(6)	100.52(7)	99.16(8)	93.31(5)	93.61(8)
N11-Fe1-N31	162.34(4)	162.18(7)	161.38(7)	164.69(7)	167.83(8)	160.32(8)	178.64(5)	174.09(7)
N21-Fe-N41	162.34(4)	162.18(7)	159.99(7)	164.69(7)	163.22(8)	172.50(8)	176.33(5)	171.65(7)
Torsions (°)								
Fe1N11-	0.62(14)	0.0(3)	3.4(3)	2.5(2)	-22.9(3)	8.2(3)	-4.2(2)	-3.1(2)
Fe1N21-	-2.96(13)	-1.7(3)	-6.2(2)	-2.5(2)	-16.0(3)	19.0(3)	-3.4(2)	-5.4(2)
Fe1N31-	2.96(13)	1.7(3)	4.1(2)	-10.7(2)	1.3(3)	8.1(3)	4.7(2)	7.9(3)
Fe1N41-	-0.62(14)	-0.0(3)	-4.7(3)	10.7(2)	10.0(3)	19.1(2)	4.1(2)	3.0(2)
Fe1N1-C2C1	-1.78(17)	-1.6(4)	0.4(3)	0.0	-10.3(3)	3.7(3)	-2.(2)	-3.1(2)
Fe1N1-C6C7	1.78(17)	1.6(4)	0.1(2)	0.0	8.4(4)	-2.2(3)	5.3(2)	5.9(2)

**Table 2-3.** Selected interatomic bond distances (Å), bond angles (°), and bond torsions (°) in **1-5**.

The structure of the cation in **5** (Figure 2-2) is distinct from those in **1-4** in the metric parameters about iron(II) as well as in the temperature dependence of the structural features. At 100 K, the average Fe-N<sub>pz</sub> bond distance of 1.961(1) Å for **5** is very short relative to the range of 2.18 to 2.28 Å found for **1-4** determined at the same temperature.

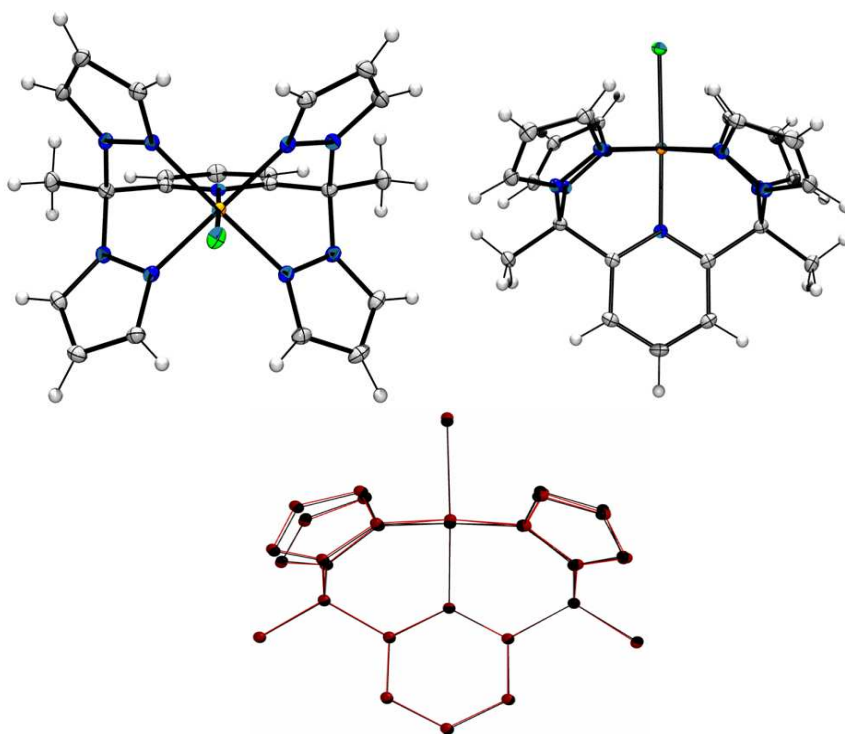


**Figure 2-2.** Left and middle: Views of the 100 K structure of the  $[\text{FeCl}(\text{pz}_4\text{depy})]^+$  cation; Right: Overlay of 296 K (red) and 100 K (black) structures.

The short average Fe-N<sub>pz</sub> distance of 1.98 Å found in **5** is in-line with that expected low-spin Fe(II). Similarly, the Fe-N<sub>py</sub> distance of 1.93 Å is significantly shorter than the range of 2.21 to 2.27 Å in **1-4** each with high-spin iron(II) and is comparable to the axial Fe-N<sub>py</sub> distance of the pentadentate ligand in  $[\text{Fe}(\text{CH}_3\text{CN})(\text{PY}5)](\text{ClO}_4)_2$ <sup>3</sup> [1.927(8) Å] or in  $[\text{Fe}(\text{py})(\text{PY}5)](\text{OSO}_2\text{CF}_3)_2$ <sup>18</sup> [1.987(8) Å] where both latter examples are authentically low-spin iron(II) complexes. The structure of **5** at 296 K differs from the 100 K structure by a small but significant lengthening of the iron-nitrogen bonds; the Fe-Cl bond distance becomes slightly shorter on warming decreasing from 2.325 Å at 100 K to 2.318 Å at 296 K, but still remains in the 2.32 to 2.35 Å range found in complexes **1-4**. In **5**, the average Fe-N<sub>pz</sub> bond distance increases by about 0.05 Å from 1.961(1)

Å at 100 K to 2.010(2) Å at 296 K whereas the Fe-N<sub>py</sub> bond increases by about 0.09 Å from 1.932(1) Å at 100K to 2.019(2) Å at 296 K. This modest bond lengthening is greater in magnitude than found in **1**. Moreover, the related [CoCl(pz<sub>4</sub>depy)(Cl)·MeOH complex crystallizes in the same C2/c space group as **5** but shows no change in the Co-N<sub>pz</sub> bond distances with temperature (Figure 2-3). Taken altogether, the significant temperature-dependent bond length changes in **5** is suggestive of the onset of an electronic spin-state change rather it than being a typical consequence of heating.

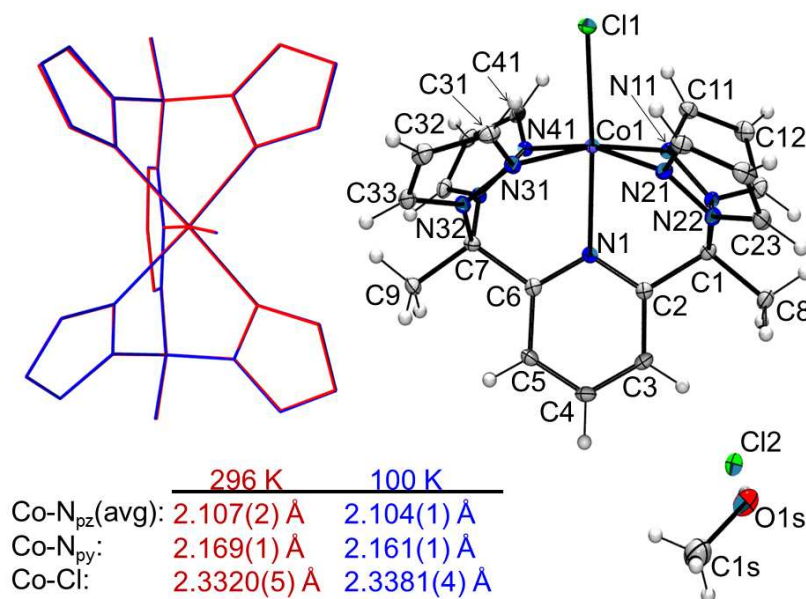


**Figure 2-3.** Structural depictions and overlays of [CoCl(pz<sub>4</sub>depy)](Cl)·MeOH, **7**·MeOH. Left: 296 K (red wireframe) and 100 K (blue wireframe) structures. Right: partial atom labeling of 100 K structure.

Closer inspection of the overlaid low- and high-temperature structures of **5** (bottom of Figure 2-2) reveals that the bond lengthening is also accompanied by small structural distortions in the cation that correlate with the ligand binding to a larger metal center upon switching from low-spin to high-spin iron(II), vide infra. The most obvious effect of the combined structural distortions is that at high temperature iron(II) is 0.124 Å above the mean plane of the four iron-bound pyrazolyl nitrogens, whereas at low temperature it is only 0.042 Å above this plane, a difference of about 0.08 Å. For perspective, in **1**·CH<sub>2</sub>Cl<sub>2</sub>, the iron(II) is high-spin and resides 0.400 and 0.392 Å above the N(pz)<sub>4</sub> plane at 270 and 100 K, respectively. Moreover, at 100 K

the iron(II) sits 0.332 and 0.336 Å above the N(pz)<sub>4</sub> plane in **1**·MeOH and **1**·2MeOH, respectively. An overlay of the cations of **1** and **5** (left of Figure 2-4) affords a classic view of the structural differences that occur for iron(II) complexes with different electronic spin states. The difference between the structures of **1** and **5** can be rationalized by the different steric demands of the methine substituent (methyl versus H, center and right of Figure 2-4). A methyl group bound to methine has modest steric requirements and can “push” against the heterocycles and favor a low spin iron(II) coordination environment, whereas a methine hydrogen does not have sufficient size to enforce a low-spin iron(II) with a nominally weak-field FeN<sub>5</sub>Cl donor set.

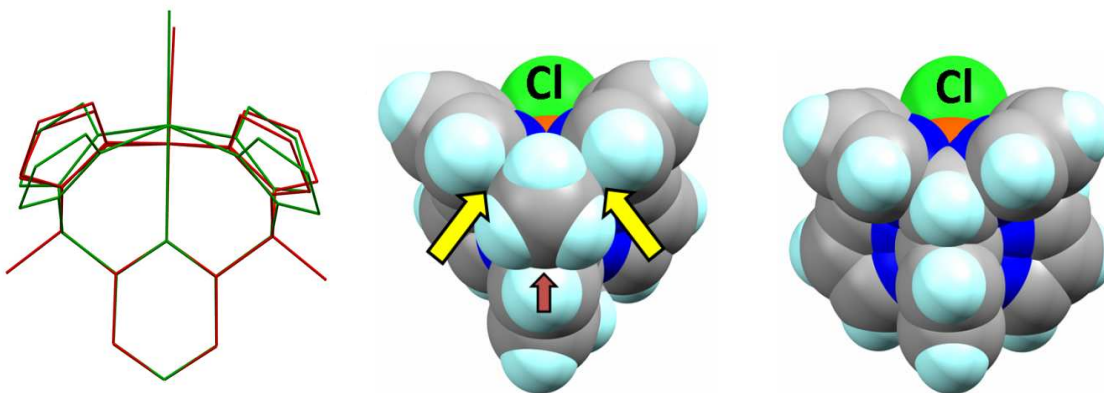


**Figure 2-4.** Left: Overlay of cation structures in **1** (green) and **5** (red); Middle and right: Side views of space-filling representations of **5** and **1**, respectively, highlighting potential steric interactions in **5**.

A more penetrating insight into the nature of the steric issues, discussed herein, that may help inform future ligand designs, may be gained by examination of the structural distortions that occur in this ligand system in analogy with the chemistry of complexes of the related poly(pyrazolyl)-based “scorpionate” ligands. If one considers the pentadentate ligands pz<sub>4</sub>lut or pz<sub>4</sub>depy to be two conjoined tripodal heteroscorpionate RC(pz)<sub>2</sub>py fragments with superimposed pyridyl ring atoms, then some of the structural distortions can be defined in a manner similar to that found in the scorpionate literature.<sup>17</sup> Scorpionate-based ligands can accommodate a broad range of metal centers in their binding pocket because of three ion-size dependent structural distortions in the ligand framework: M-N bond lengthening, methine pyramidalization, and ring twisting, see Figure 2-5. One understandable way that the ligands can bind relatively large

metals is by adopting longer M-N bonds and this effect is easily measurable. In the methine pyramidalization distortion, the “mouth” of the ligand is opened to accommodate larger metals while maintaining fixed  $C_{\text{meth}}-C_{\text{ipso}}-\text{N}$  or  $C_{\text{meth}}-\text{N}-\text{N}$  angles, as exaggerated by the illustration in the center of Figure 2-5. This distortion is best measured by the perpendicular distance between the central methine carbon atom and the mean plane of the two pyrazolyl nitrogens and the *ipso*-pyridyl carbon atom bound to the methine,  $\perp C_{\text{meth}}-\text{N}_2\text{C}$ , where smaller distances indicate more pyramidal carbon.

**Figure 2-5.** Main structural distortions for heteroscorpionate,  $\text{RCpz}_2\text{py}$ , fragments that occur upon binding metal cations of different size. R is H or an organic substituent while C-N and N-N represent the pyridyl and pyrazolyl rings, respectively.

In the case of  $\mathbf{5} \cdot \text{MeOH}$ ,  $\perp C_{\text{meth}}-\text{N}_2\text{C}$ , averages 0.53 and 0.52 Å at 100 and 296 K for low spin iron(II). For comparison,  $\perp C_{\text{meth}}-\text{N}_2\text{C}$ , averages 0.45 Å for  $\mathbf{1}$  with high-spin iron(II), independent of included solvent and temperature. Greater pyramidalization contributes, in part, to an increase in the average non-bonded contact distance between the three metal-binding nitrogen atoms,  $(\text{N} \cdots \text{N})_{\text{avg}}$ , a measure used by Sohrin<sup>26</sup> and others<sup>27</sup> to indicate ligand “bite” size. If the metal ion or the steric demand of the organyl at the ‘back’ position R of the heteroscorpionate is too large, scorpionate ligand binding is accompanied by ring twisting, as in the right of Figure 2-5. This distortion is best measured by the  $\text{MN}-(\text{E})\text{C}_{\text{methine}}$  torsion angle where E is either N or C depending on whether the ring is a pyrazolyl or a pyridyl, respectively. A complex with “non-twisted” rings has  $\text{MN}-(\text{E})\text{C}_{\text{methine}}$  torsion angles of  $0^\circ$ ; typically the “twist” torsion angles are finite but are less than  $\sim 20^\circ$  for low-spin iron(II) complexes. The ring twisting distortion contributes to increasing  $(\text{N} \cdots \text{N})_{\text{avg}}$  and also shows a small dependence on crystal

packing.<sup>28</sup> For the low-spin iron(II) in **5**·MeOH at 100 K, (N...N)<sub>avg</sub> is 2.715(1) Å, a distance which increases by 0.042 Å to 2.757(2) Å at 296 K. The value of (N...N)<sub>avg</sub> for **1** with high spin iron(II) is in the narrow range of 2.88 to 2.90 Å regardless of solvent of crystallization or temperature; only a 0.007 Å difference in (N...N)<sub>avg</sub> occurs in the 100 and 270 K structures of **1**·CH<sub>2</sub>Cl<sub>2</sub>. Generally, there is a smaller ligand bite and less ligand distortions for low spin Fe(II) complexes than for the relatively larger high spin iron(II) complexes. The judicious choice of substituents along the ligand periphery to manipulate distortions may be an important key for controlling the electronic spin state and coordination preferences. In **5**·MeOH the presence of the methyl group bound to the methine hinders the pyramidalization without drastically altering the pyrazolyl ring twisting. It is expected that larger groups, i.e, i-Pr, t-Bu, or Ph, bound to the methine carbon would enforce more extensive ring-twisting and might even change the coordination environment about the iron(II) ion, as is found in the related iron(II) poly(pyrazolyl)borate systems; this hypothesis is currently under investigation for pz<sub>4</sub>lut-type variants.

As a final note, the solids obtained directly from the preparative reactions of **1-5** are microcrystalline as determined by powder X-ray diffraction measurements. For **5**, the experimental powder X-ray diffraction patterns of the microcrystalline precipitates match those calculated from the single crystal structural data indicating that the single crystals appear to be representative of the bulk samples (see Figure 2-6).

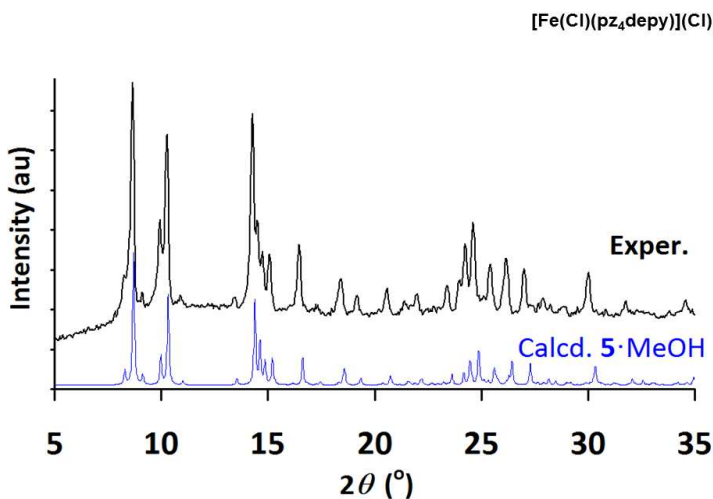


**Figure 2-6.** Calculated (blue, bottom) and observed (black, top) PXRD data for **5**·MeOH.



**Solution Properties.** In a fashion similar to that reported previously for **1**·CH<sub>2</sub>Cl<sub>2</sub>, the paramagnetic NMR spectra of each complex **1-4** in methanol and their 295 K solution magnetic moments  $\mu_{\text{eff}}$  5.2-5.6  $\pm$  0.3  $\mu_{\text{B}}$  (Evan's) are typical of high-spin iron(II) complexes. However, the observed 295 K solution  $\mu_{\text{eff}}$  values of 2.9 and 1.9  $\mu_{\text{B}}$  for **5** and **6**, respectively, are much lower than expected for high-spin iron(II). Therefore, the temperature dependence of the magnetic moment of each **5** and **6** in CD<sub>3</sub>OD was measured between 213 K and 313 K and was found to be characteristic of an incomplete electronic spin-state crossover, see Figure 2-7. If one considers unquenched orbital angular momentum, the reference temperature,  $T_{1/2}$ , where the sample is 50% high-spin iron(II) ( $\mu_{\text{eff}} \approx 2.74 \mu_{\text{B}}$ ), is estimated to be ca. 295 and 315 K for **5** and for **6**, respectively.

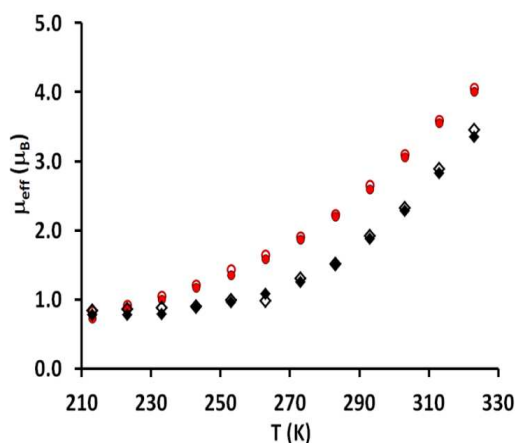


**Figure 2-7.** Temperature dependence of the magnetic moment of **5** (red, higher trace) and **6** (black, lower trace) in MeOH.

Another possible explanation for the rise in magnetic moment of the solution with temperature is that the chloro ligand separates from the metal upon warming. It is known that ligands are always in equilibrium with a metal donor in solution. The monodentate chloro ligand is much more likely to dissociate from the metal than the pentadentate ligand due to the predicted stability constants. The magnitude of the stability constant of the complex determines how tightly bound the ligand(s) are to the metal. The stability constant of the pentadentate ligand should be

much higher than that of the monodentate ligand, (see Chapter 1). The latter stability constant in methanol has not yet been determined.

The colors of the complexes vary depending on the presence (or absence) and position of methyl substituents. As solids, **1** is orange-yellow, **2** is orange, **3** and **4** are both yellow with **3** being brighter yellow compared to **4**, **5** is deep red-orange, and **6** is rose-red, see Figure 2-8. For the most part, the colors of methanol solutions of the complexes resemble those in the solid state giving qualitative evidence that the complexes remain intact in methanol.



**Figure 2-8.** Photograph of samples complexes **1-6**.

An exception occurs for complex **6** which forms a deep orange solution in methanol (orange-brown when concentrated) rather than the solid-state rose-red color or the pink-red color that is characteristic of its dichloromethane solutions. Quantitative evidence for solution-phase complex formation and information regarding the electronic properties of the complexes were obtained from electronic absorption spectral data. Job's method was utilized to confirm the 1:1 stoichiometric ratio between the ligand and the metal for complexes **1-5** (see Figure 2-9).

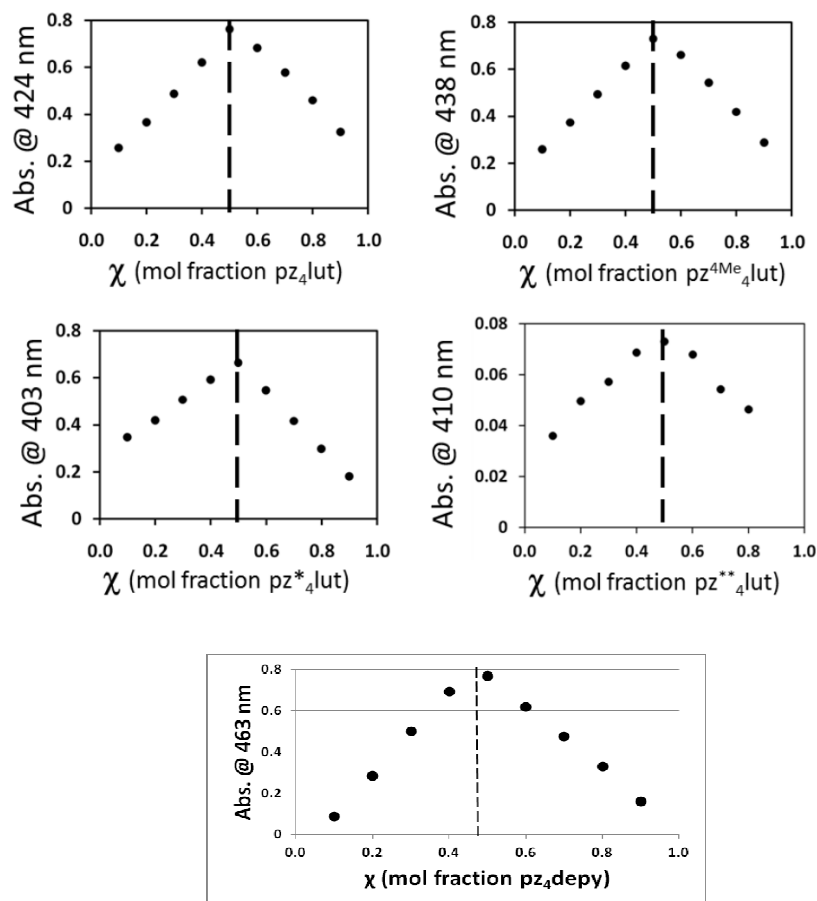


**Figure 2-9:** Jobs Plots for complexes 1-5.

An overlay of the low energy portion of the UV-spectra of methanol solutions of **1-4** are provided in Figure 2-10. The spectra of **1-4** are comprised of four main bands. There are two higher-energy bands near  $\lambda_{\text{max}} = 200$  ( $\epsilon \sim 10^4 \text{ M}^{-1}\text{cm}^{-1}$ ) and  $\lambda_{\text{max}} = 254$  nm ( $\epsilon \sim 10^3 \text{ M}^{-1}\text{cm}^{-1}$ ), respectively that may presumably be assigned to intra-ligand  $\pi\text{-}\pi^*$  or  $\text{n-}\pi^*$  transitions or perhaps metal to ligand charge transfer  $3\text{d}_{\text{Fe}}$  to  $\pi^*(\text{py})$  transitions based on their energies and intensities and comparisons with the spectra for the free ligands and related complexes. There is also a medium-energy, lower-intensity band near 450 nm ( $\epsilon \sim 10^2\text{-}10^3 \text{ M}^{-1}\text{cm}^{-1}$  depending on the complex) that is tentatively assigned as a  $(\text{p}\pi(\text{Cl}) \rightarrow \text{Fe d}\pi)$  ligand to metal charge transfer (LMCT) band based on a comparison with the spectrum of  $\text{FeCl}_2$  and with literature assignments for related complexes.<sup>19</sup>

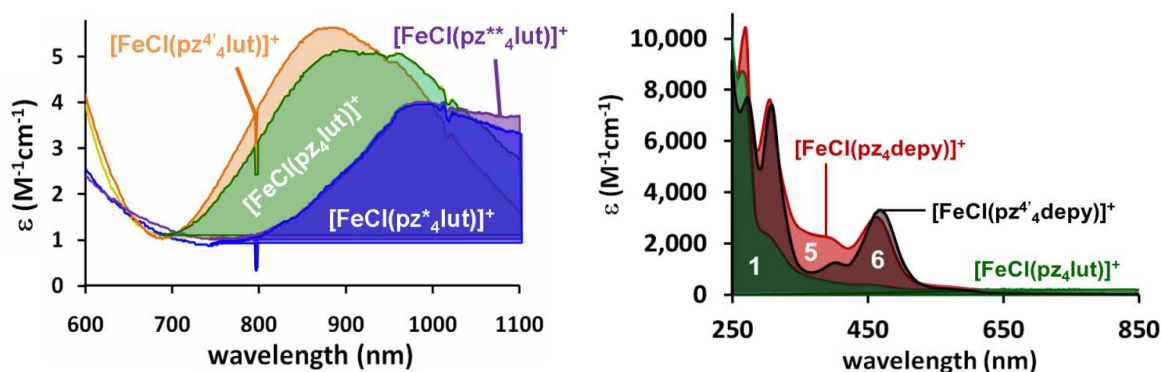


**Figure 2-10.** Left: Overlay of the d-d region of the spectrum of each **1** (green), **2** (orange), **3** (blue), and **4** (violet) in MeOH (Reproduced from Reference 9); Right: Overlay of electronic absorption spectrum of **1** (green), **5** (red) and of **6** (black) in MeOH.

This LMCT band gives rise to the observed colors of the complexes and the low-energy edge progressively penetrates from the violet region of the electromagnetic spectrum for **4** and **3** into the lower energy (blue) region for **1** and **2**. Finally, there is a very weak-intensity band ( $\epsilon \sim 10^2 M^{-1}cm^{-1}$ ), or set of split bands due to the  $C_{4v}$  local symmetry, found in the near-IR region at  $\lambda_{max} \sim 900$  nm for **1** and **2** and at  $\lambda_{max} \sim 1000$  nm for **3** and **4**. These bands are characteristic of *d-d* transition(s) associated with high-spin iron(II) ions. An estimate of  $10 Dq$  for the four complexes obtained by using the average of the *d-d* bands yields 10,400, 11,000, 9,700, and 9,800  $cm^{-1}$  for **1-4**, respectively. These values indicate that 3-methylpyrazolyl substitution (as in the cases of **3** and **4**) resulted in ligands with a weaker crystal field compared to those with hydrogens at the 3-position of the pyrazolyls (as in the cases of **1** and **2**). This observation is also in accord with the steric arguments presented above. In contrast, replacing the hydrogen with a methyl at the 4-position of a pyrazolyl (as in the cases of **2** and **4**) modestly increases the ligand crystal field strength in the expected manner by increasing the ligands'  $\pi$ -donor abilities through inductive effects. The electronic absorption spectra of **5** and **6** in methanol (right of Figure 2-9) are similar to those of **1-4** but the medium-energy bands between 300 to 450 nm are much more intense for **5** and **6** than for the latter. Also, the expected *d-d* transitions in **5** and **6** for low-spin or high-spin iron(II) were not observed as they are likely masked by charge transfer transitions or, considering the small fraction of high-spin iron(II) present in the solution and the small magnitude of the extinction coefficient, by the unfavorable signal-to-noise. It is noteworthy that the isomolar

titration data (Job's Plots, ca.  $10^{-3}$  M in MeOH) obtained by monitoring the change in absorbance of the charge-transfer bands near 400 to 450 nm confirmed that complexes with 1:1  $\text{FeCl}_2\text{:pz}^{\text{R}}_4\text{lut}$  stoichiometry are formed immediately in solution upon mixing reagents.

**Electrochemistry.** A comparison of the cyclic voltammograms (100 mV/s) of the crystalline complexes dissolved in deaerated MeOH with  $(\text{NBu}_4)(\text{HSO}_4)$  as a supporting electrolyte is found in Figure 2-11. Each iron complex exhibits an irreversible or quasi-reversible oxidation wave between ca. 0.95 to 0.75 V versus Ag/AgCl.

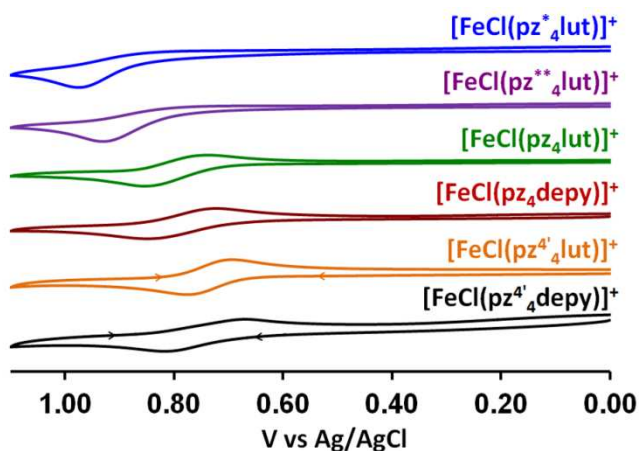


**Figure 2-11.** Cyclic voltammograms of the iron(II) chloride complexes of  $\text{pz}^{\text{R}}_4\text{lut}$  and  $\text{pz}^{\text{R}}_4\text{depy}$  in MeOH obtained at 100 mV/s with  $(\text{NBu}_4)(\text{HSO}_4)$  as the supporting electrolyte.

Comparison of current intensities with equimolar mixtures of complexes **1-6** and ferrocene ( $E_{1/2} = 0.47$  V) as well as spectrophotometric titrations of each complex with Magic Blue indicate the oxidation of each complex is a one-electron event. Although the irreversible nature of the oxidations of **3** and **4** prohibit unambiguous determination of  $E_{1/2}$  values, the relative anodic potentials indicate, as expected, that the stronger field ligands generally give less positive redox potentials, i.e., are easier to oxidize.

## 2-5 Conclusions:

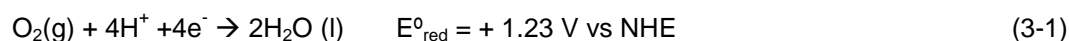
The systematic introduction of methyl groups along the periphery of the tetra(pyrazolyl)lutidine ligand framework provides a simple means to alter their apparent ligand

field strength, as has been gauged by the properties of their iron(II) chloride complexes. Derivatives with methyl groups at the 3-pyrazolyl position reduce the field strength via intra- and inter-ligand steric interactions whereas substitution at the 4-pyrazolyl position increases ligand field strength, although not enough to yield low spin iron(II). On the other hand, placing methyl groups at the methine carbon positions provides access to iron(II) complexes that undergo spin-state change ( $T_{1/2} \sim 300\text{K}$ ) and that are fully low spin below 210 K in the solid state and in solution. The substantial increase in ligand field strength versus derivatives with hydrogen at the methine carbons is attributed to the modest steric interactions between the methyl groups and neighboring heterocyclic rings that favor a smaller ligand bite without requiring pyrazolyl ring distortion that would lead to longer Fe-N bonds. Since it was shown that substitution at the 4-pyrazolyl position causes a slight increase in  $T_{1/2}$  and that it is known that changes in anion, solvent, or ligand substituents can provoke significant changes in spin crossover behavior in other iron(II) systems,<sup>20</sup> complexes of  $\text{pz}^{\text{R}}_4\text{depy}$  variants will be researched in due course. Importantly, the ability to use simple reactions to modify the  $\text{pz}^{\text{R}}_4\text{lut}$  framework and to traverse spin states of iron(II) opens the door for numerous avenues of study including examination of any spin-state dependent reactivity of importance in biological or synthetic systems.

## Chapter 3: Aquacobalt(II) complexes of pz<sub>4</sub>depy

### 3-1 Introduction:

There have been rapidly growing efforts to address current and emergent energy and environmental challenges occurring from the use of the limited supply of fossil fuels. The possibility of using water as an alternative, abundant, and clean fuel source is attractive from many standpoints. However, the decomposition of water into its constituent elements to be used as fuels is a formidable task given the high enthalpy of formation ( $\Delta H_f \text{H}_2\text{O (g)} = -241.8 \text{ kJ/mol}$ ) and free energy of formation ( $\Delta G_f \text{H}_2\text{O (g)} = -228.6 \text{ kJ/mol}$ ).<sup>1</sup> Also, this reaction requires shuttling multiple equivalents of protons and electrons in accord with the two half reactions (in acidic solution) in Equations 3-1 and 3-2 below:



It has long been known that  $\text{Co}^{3+}$  ions are highly oxidizing ( $E^\circ_{\text{red}}(\text{Co}^{3+}/\text{Co}^{2+}) = +1.82 \text{ V vs NHE}$ ). Thus, there have been several reports on the use of various heterogeneous water oxidation catalysts (WOC) based on insoluble inorganic cobalt salts.<sup>2-5</sup> At the beginning of this research, there was a seminal report by the Berlinguette group that describes a homogeneous WOC based on  $[(\text{PY}5)\text{Co}(\text{H}_2\text{O})]^{2+}$  (herein referred to as **1**).<sup>6</sup> This report was significant since most other known homogeneous WOC's were based on expensive heavy metal complexes such as Ru,<sup>7</sup> Ir,<sup>8</sup> and Re.<sup>9</sup> Given the similarities between our pz<sub>4</sub>depy and pz<sub>4</sub>lut ligands and PY5 derivatives, we sought to determine how cobalt complexes based on our ligand systems compared with the PY5 derivatives in terms of their electronic properties and possibly, water oxidation behavior. To this end, we established a collaboration with the Berlinguette group at the University of Calgary. They performed advanced electrochemical measurements, including water-oxidation experiments. This chapter will describe our efforts in the synthesis and characterization of the complexes. The findings from the Berlinguette group are also summarized below. Full details regarding the advanced electrochemical studies are found in the literature.<sup>10,11</sup>

### 3-2 Synthesis:

**General Considerations.** The ligand pz<sub>4</sub>lut was prepared as described in chapter 2. The complex [Co(H<sub>2</sub>O)<sub>6</sub>](OTs = p-O<sub>3</sub>SC<sub>6</sub>H<sub>4</sub>CH<sub>3</sub>)<sub>2</sub> was prepared by a literature procedure.<sup>12</sup> [Co(H<sub>2</sub>O)<sub>6</sub>](ClO<sub>4</sub>)<sub>2</sub> was used as received from a commercial source. *Caution:* Although we did not encounter any problems, perchlorate salts of metal complexes are potentially explosive. Only small quantities of the compound should be prepared and handled with care.

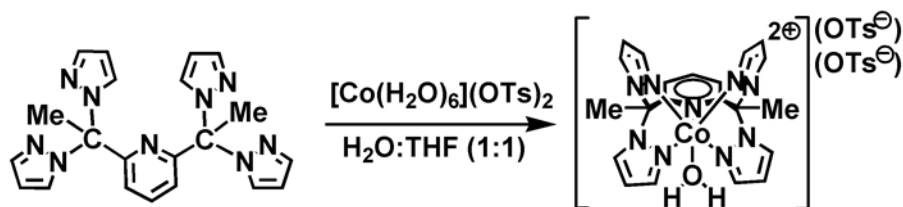
**Improved synthesis of pz<sub>4</sub>depy.** Although the synthesis of the pz<sub>4</sub>depy ligand is reported in the previous chapter, an easier, higher yielding preparation was found as described below.

**pz<sub>4</sub>depy.** Under a nitrogen blanket, a solid portion of 0.682 g (6.08 mmol) K(t-BuO) was added to a solution of 0.752 g (2.02 mmol) pz<sub>4</sub>lut in 25 mL THF. The reaction mixture turned orange immediately upon mixing and was allowed to stir at room temperature for 30 min. Then, 0.38 mL (0.86 g, 6.1 mmol) CH<sub>3</sub>I was added by syringe, forming a colorless precipitate. After the reaction mixture had been stirred for an additional 90 min, 25 mL each of water and Et<sub>2</sub>O were added sequentially. The organic and aqueous layers were separated, and the aqueous layer was extracted with two 25 mL portions of Et<sub>2</sub>O. The combined organic fractions were dried over MgSO<sub>4</sub>, filtered, and solvent was removed to leave a colorless solid with a small amount of yellow oil. The yellow oil was removed by trituration with 5 mL Et<sub>2</sub>O, decanting the yellow solution, and drying the product at room temperature under vacuum for 30 min to afford 0.710 g of colorless solid (88 % based on pz<sub>4</sub>lut). The characterization data are the same as previously reported: Mp, 157-159°C. <sup>1</sup>H NMR (CDCl<sub>3</sub>): δ 7.65 (t, J = 7.8 Hz, 1H, H<sub>4-py</sub>), 7.61 (d, J = 2 Hz, 4H, H<sub>3-pz</sub>), 7.13 (d, J = 1 Hz, 4H, H<sub>5-pz</sub>), 6.45 (d, J = 7.8 Hz, 2H, H<sub>3,5-py</sub>), 6.27 (dd, J = 1; 2 Hz, 4H, H<sub>4-pz</sub>), 2.65 (s, 6H, CH<sub>3</sub>). <sup>13</sup>C NMR (CDCl<sub>3</sub>): δ 159.1, 140.3, 138.5, 129.6, 121.1, 106.1, 82.5, 26.4.

**[Co(H<sub>2</sub>O)(pz<sub>4</sub>depy)](ClO<sub>4</sub>)<sub>2</sub>, [2](ClO<sub>4</sub>)<sub>2</sub>.** A mixture of 0.297 g (0.744 mmol) pz<sub>4</sub>depy, 0.272 g (0.743 mmol) [Co(H<sub>2</sub>O)<sub>6</sub>](ClO<sub>4</sub>)<sub>2</sub>, 5 mL of THF and 5 mL of de-ionized H<sub>2</sub>O was heated at reflux for 5 min. to give a yellow solution. After cooling to 50°C with an external water bath, the solvents were removed under vacuum (1x10<sup>-3</sup> torr) to leave 0.470 g of [2](ClO<sub>4</sub>)<sub>2</sub> (94% based on



cobalt) as a pale yellow solid. Heating a mixture of 0.36 g of the pale yellow solid in 20 mL H<sub>2</sub>O to reflux gave a solution that, after cooling to room temperature over 2 h, deposited 0.27 g of X-ray quality yellow blocks (solubility at 22°C 0.10 g/20 mL or 7.4 mM) which were collected by vacuum filtration and air dried. A second crop of crystals (0.04 g) were obtained by concentrating the mother liquor to 5 mL. The characterization data are for the crystalline sample. Mp, 225 °C (decomp. to pale orange solid that remains unchanged to 300°C). Anal. Calcd. (obsd.) for C<sub>21</sub>H<sub>23</sub>Cl<sub>2</sub>CoN<sub>9</sub>O<sub>9</sub>: C, 37.35 (36.98); H, 3.43 (3.41); N, 18.67(18.42).  $\mu_{\text{eff}}$  (solid, 295 K): 4.46  $\mu_B$ . UV-Vis (H<sub>2</sub>O)  $\lambda_{\text{max}}$ , nm ( $\epsilon$ , M<sup>-1</sup>cm<sup>-1</sup>): 205 sh (30,000), 211 sh (24,000), 261 (4,400), 459 (24), 510 sh (8), 758 sh (4), 871 sh (7), 961 (17).



**Scheme 3-1.** Metallation of [Co(H<sub>2</sub>O)<sub>6</sub>](OTs)<sub>2</sub> with pz<sub>4</sub>depy.

**[Co(H<sub>2</sub>O)pz<sub>4</sub>depy](OTs)<sub>2</sub>•2H<sub>2</sub>O. [2](OTs)<sub>2</sub>•2H<sub>2</sub>O.** A colorless solution of 0.252g (0.631 mmol) pz<sub>4</sub>depy in 5 mL of THF was added via cannula transfer to a pink solution of 0.291 g (0.630 mmol) [Co(H<sub>2</sub>O)<sub>6</sub>](OTs)<sub>2</sub> in 5 mL of de-ionized H<sub>2</sub>O, which gave a yellow solution upon complete mixing. After stirring 5 min, solvents were removed under vacuum via rotary evaporation. The resulting orange solid was triturated with hot acetone to give a pale yellow powder of the desired product that was isolated after decanting the acetone solution and drying the remaining solid under vacuum. The pale yellow solid was recrystallized by dissolution in minimal (ca. 2 mL) H<sub>2</sub>O and allowing the solution to cool to room temperature over the course of several hours. In this way, large yellow crystals of **2**•3H<sub>2</sub>O suitable for X-ray diffraction are obtained. Drying the crystals under vacuum causes the crystals to desolvate and shatter into 0.372g (69% based on cobalt) of **[2](OTs)<sub>2</sub>•2H<sub>2</sub>O** as a pale orange powder. Mp, 135 – 137 °C (decomp. to orange residue with apparent gas evolution). Anal. Calcd. (obsd.) for **[2](OTs)<sub>2</sub>•2H<sub>2</sub>O**, C<sub>35</sub>H<sub>41</sub>CoN<sub>9</sub>O<sub>9</sub>S<sub>2</sub>: C, 49.17 (49.27); H, 4.83 (4.45); N, 14.75(14.72).  $\mu_{\text{eff}}$  (solid,

297 K):  $4.4 \pm 0.1 \mu_B$ . UV-Vis (H<sub>2</sub>O)  $\lambda_{\max}$ , nm ( $\epsilon$ , M<sup>-1</sup>cm<sup>-1</sup>): 221 (51,200), 262 (5,600), 458 (28), 508 sh (11), 862 (6), 935 (6).

### 3-3 Crystallographic Structure Determinations:

X-ray intensity data from a yellow block of [2](ClO<sub>4</sub>) and a yellow plate of [2](OTs)2•3H<sub>2</sub>O were collected at 101.1 K with an Oxford Diffraction Ltd. Supernova diffractometer equipped with a 135 mm Atlas CCD detector using Mo(K $\alpha$ ) for the former crystal but Cu(K $\alpha$ ) radiation for the latter. Raw data frame integration and Lp corrections were performed with CrysAlis Pro (Oxford Diffraction, Ltd.)<sup>13</sup> Final unit cell parameters were determined by least-squares refinement of 5960 and 10696 reflections from the data sets of [2](ClO<sub>4</sub>) and [2](OTs)2•3H<sub>2</sub>O, respectively, each with  $I > 2\sigma(I)$ . Analysis of the data showed negligible crystal decay during collection in each case. Direct methods structure solutions, difference Fourier calculations and full-matrix least-squares refinements against F<sup>2</sup> were performed with SHELXL-97.<sup>14</sup> An empirical absorption correction was applied to the data of [2](ClO<sub>4</sub>) using spherical harmonics implemented in the SCALE3 ABSPACK multi-scan method.<sup>15</sup> A numerical absorption correction based on Gaussian integration over a multi-faceted crystal model was applied to the data of [2](OTs)2•3H<sub>2</sub>O. In the structure of [2](ClO<sub>4</sub>) the iron-bound water molecule appears to be very slightly disordered about the two-fold axis which gives rise to the elongated ellipsoid for O1w. The structure of [2](OTs)2•3H<sub>2</sub>O contains several symmetry-inequivalent moieties in the asymmetric unit, including: two dications, four anions, and six solvated water molecules. There is extensive disorder of the anions and three of the solvate water molecules partially populated among at least two positions each. The carbon atoms of disordered p-toluenesulfonate ions were refined isotropically. All other non-hydrogen atoms in each structure were refined with anisotropic displacement parameters. Since the positions of hydrogen atoms on the partially occupied disordered water molecules in [2](OTs)2•3H<sub>2</sub>O could not be satisfactorily modeled, they were omitted from the refinement. All other hydrogen atoms in each structure were placed in geometrically idealized positions and were included as riding atoms. Further details of the refinement can be found in Table 3-1.

Compound	[2](ClO <sub>4</sub> ) <sub>2</sub>	[2](OTs) <sub>2</sub> •3H <sub>2</sub> O
Formula	C <sub>21</sub> H <sub>23</sub> Cl <sub>2</sub> CoN <sub>9</sub> O <sub>9</sub>	C <sub>35</sub> H <sub>40</sub> CoN <sub>9</sub> O <sub>10.02</sub> S <sub>2</sub>
Formula weight	675.31	870.21
Crystal system	monoclinic	Monoclinic
Space group	C 2/c	P 2/c
Temp. [K]	101.7	101.1
a [Å]	21.0799(13)	30.9019(10)
b [Å]	12.0108(5)	12.4380(3)
c [Å]	12.4853(8)	21.0739(6)
α [°]	90.00	90.00
β [°]	119.604(8)	108.631(4)
γ [°]	90.00	90.00
V [Å <sup>3</sup> ]	2748.5(3)	7675.4(4)
Z	4	8
D <sub>calcd.</sub> [gcm <sup>-3</sup> ]	1.632	1.506
λ [Å] (Mo Kα or Cu Kα)	0.7107	1.5418
μ [mm <sup>-1</sup> ]	0.886	5.119
Abs. Correction	multi-scan	Numerical
F(000)	1380	3618
2θ range [°]	6.74 to 59.2	7.10 to 148.00
Reflections collected	15895	42973
Independent reflections	3518[R(int) = 0.0330]	15195[R(int) = 0.0322]
T <sub>min</sub> /max	0.92954/1.00000	0.556/0.787
Data/restraints/ parameters	3518/0/197	15195/94/1214
Goodness-of-fit on F <sup>2</sup>	1.075	1.017
R1/wR2[ I >2σ(I)] <sup>a</sup>	0.308/0.0675	0.0536/0.1322
R1/wR2 (all data) <sup>a</sup>	0.0413/0.0744	0.0688/0.1428
Largest diff. peak/hole/ e Å <sup>-3</sup>	0.380/-0.520	0.877/-0.656

**Table 3-1.** Crystallographic data collection and structure refinement for [2](ClO<sub>4</sub>) and [2](OTs)<sub>2</sub>•3H<sub>2</sub>O. <sup>a</sup>  $R1 = \sum ||Fo| - |Fc|| / \sum |Fo|$   $wR2 = [\sum w(|Fo| - |Fc|)^2 / \sum w|Fo|^2]^{1/2}$ .

### 3-4 Calculations:

DFT calculations were performed with the M06 meta-hybrid GGA functional<sup>16</sup> using the Def2-SV(P) double-zeta basis set.<sup>17</sup> Solvent (H<sub>2</sub>O) effects were accounted for by using the polarizable continuum model IEFPCM,<sup>18</sup> as implemented in Gaussian 09.<sup>19</sup> The current model was chosen owing to its computationally inexpensive nature and its superior performance over other combinations of functionals (M06 or B3LYP<sup>20,21</sup>) and basis sets (Def2-SV(P) or 6311-G\*/LANL2DZ<sup>22-24</sup>) for reproducing bond distances and spectroscopic data, see Table 3-2.

<i>Distances (Å)</i>	[(PY5)Co(H <sub>2</sub> O)] <sup>2+</sup>		[(pz <sub>4</sub> depy)Co(H <sub>2</sub> O)] <sup>2+</sup>			
	Calcd.	Exper. <sup>a</sup>	Calcd.	Exper. <sup>b</sup>	Exper. <sup>c</sup>	Exper. <sup>a</sup>
Co-O	2.072	2.027	2.053	2.044	2.032	2.013
Co-N <sub>py</sub>	2.086	2.090	2.136	2.132	2.135	2.120
Co-N <sub>eq</sub>	2.209	2.211	2.111	2.103	2.100	2.106
Co-N <sub>eq</sub>	2.208	2.168	2.111	2.101	2.098	2.106
Co-N <sub>eq</sub>	2.132	2.134	2.11	2.101	2.096	2.087
Co-N <sub>eq</sub>	2.131	2.124	2.109	2.091	2.094	2.087
avg. Co-N <sub>ax</sub> O	2.079	2.059	2.095	2.088	2.084	2.067
avg. Co-N <sub>eq</sub>	2.170	2.159	2.110	2.099	2.097	2.097
avg. Co-N <sub>all</sub>	2.153	2.145	2.115	2.106	2.105	2.101
avg. Co-N <sub>5</sub> O	2.140	2.126	2.105	2.095	2.093	2.087
<i>Angles (°)</i>						
C <sub>p</sub> -N <sub>py</sub> -Co <sup>d</sup>	152.9	159.2	175.8	171.5	171.0	180.0
avg. ring twist <sup>e</sup>	8.5	9.0	4.0	8.0	8.6	1.6
<sup>mpin</sup> py- <sup>mpin</sup> N <sub>4</sub> <sup>†</sup>	63.1	69.6	85.7	81.1	80.7	90.0

**Table 3-2:** Comparison of calculated (M06/Def2-SV(P)) versus experimental bond distances and angles in [(PY5)Co<sup>II</sup>(H<sub>2</sub>O)]<sup>2+</sup> and [(pz<sub>4</sub>depy)Co<sup>II</sup>(H<sub>2</sub>O)]<sup>2+</sup> (<sup>a</sup> ClO<sub>4</sub><sup>-</sup>; <sup>b</sup> OTs<sup>-</sup>, 1st independent unit; <sup>c</sup> OTs<sup>-</sup>, 2nd independent unit; <sup>d</sup> C<sub>p</sub> = carbon para- to N on axial pyridine ring; <sup>e</sup> defined as the absolute value of C<sub>methine</sub>N<sub>pz</sub>-N<sub>pz</sub>Co or C<sub>methine</sub>C<sub>py</sub>-N<sub>py</sub>Co torsion angle (six such angles per complex); <sup>†</sup> dihedral angle between mean plane of the axial pyridyl ring and the mean plane of the four equatorial cobalt-bound nitrogen atoms.)

For [(L)Co(OH<sub>x</sub>)]<sup>z+</sup> (x = z=1, 2), calculations were performed for high spin (2S+1 = 4) states as found experimentally. Calculations for the cobalt(III) species were performed only considering low spin (2S+1 = 1) states. Analytical vibrational frequency calculations were also carried out to verify that the optimized geometries were stationary points. A more thorough computational study using higher quality computational models and considering all possible spin multiplicities is underway.

### 3-5 Results and Discussion:

An improved preparation of the pz<sub>4</sub>depy ligand has been found that uses (excess) K<sup>t</sup>BuO as a base to deprotonate the methines on the pz<sub>4</sub>lut ligand prior to reaction with iodomethane. In the previous preparation, <sup>n</sup>BuLi was used as the base, which required stoichiometric quantities of base and rigorous exclusion of air and moisture. This method was also lower-yielding. The new preparation produced higher yields in shorter periods of time with a more easily handled solid

reagent. The reaction of pz<sub>4</sub>depy with either [Co(H<sub>2</sub>O)<sub>6</sub>](OTs)<sub>2</sub> or [Co(H<sub>2</sub>O)<sub>6</sub>](ClO<sub>4</sub>)<sub>2</sub> produces the desired yellow [Co(H<sub>2</sub>O)(pz<sub>4</sub>depy)](X = ClO<sub>4</sub> or OTs)<sub>2</sub> complexes in high yield. The tosylate derivative has noticeably greater solubility in water than the perchlorate. Both were recrystallized by cooling concentrated aqueous solutions to room temperature. The structures and associated bond metrics of the complexes are given in Figures 3-1 and 3-2.

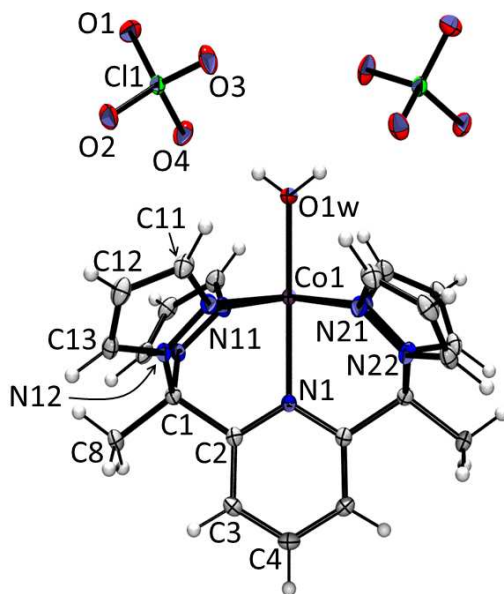


**Figure 3-1.** View of the structure of [2](ClO<sub>4</sub>) with partial atom labeling. The dication resides on a two-fold axis of rotation. Selected bond distances (Å): Co1-O1W, 2.013(2); Co1-N1, 2.1201(19); Co1-N11, 2.1055(14); Co1-N21, 2.0874(15); Selected interatomic angles (°): O1W-Co1-N1, 180.000(1); N11-Co1-N11, 171.92(8); N11-Co1-N21, 83.17(6); N11-Co1-N21', 96.07(6); N21-Co1-N21, 169.22(8); N1-Co1-N11, 85.96(4); N1-Co1-N21, 84.61(4); O1W-Co1-N11, 94.04(4); O1W-Co1-N21, 95.39(4).

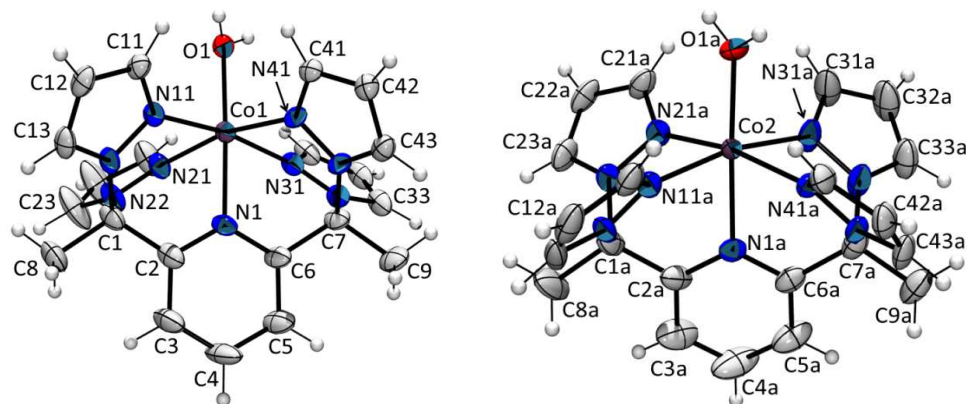


**Figure 3-2.** View of the two dications in  $[\text{Co}(\text{H}_2\text{O})(\text{pz}_4\text{depy})](\text{OTs})_2 \cdot 3\text{H}_2\text{O}$ ,  $2 \cdot 3\text{H}_2\text{O}$ .

Selected Bond Distances (Å)			
Co1-O1	2.044(2)	Co2-O1a	2.032(3)
Co1-N1	2.132(2)	Co2-N1a	2.135(2)
Co1-N11	2.091(2)	Co2-N11a	2.094(2)
Co1-N21	2.102(2)	Co2-N21a	2.098(2)
Co1-N31	2.101(2)	Co2-N31a	2.100(3)
Co1-N41	2.101(2)	Co2-N41a	2.096(2)
Selected interatomic angles (°)			
O1-Co1-N1	178.18(9)	O1a-Co2-N1a	177.60(10)
N11-Co1-N31	170.05(10)	N11a-Co2-N31a	168.46(12)
N21-Co1-N41	166.83(10)	N21a-Co2-N41a	169.65(10)
N11-Co1-N21	85.08(9)	N11a-Co2-N21a	84.39(10)
N21-Co1-N31	93.75(9)	N21a-Co2-N31a	95.67(11)
N31-Co1-N41	84.82(9)	N31a-Co2-N41a	84.61(11)
N41-Co1-N11	93.41(9)	N41a-Co2-N11a	93.27(10)
N1-Co1-N11	85.23(9)	N1a-Co2-N11a	84.78(10)
N11-Co1-O1	93.35(9)	N11a-Co2-O1a	96.27(12)

**Table 3-3:** Selected structural parameters of the two dications in  $[\text{Co}(\text{H}_2\text{O})(\text{pz}_4\text{depy})](\text{OTs})_2 \cdot 3\text{H}_2\text{O}$ ,  $2 \cdot 3\text{H}_2\text{O}$ .

The metric parameters about each cation are nearly identical. A comparison of solid state structures of PY5 and  $\text{pz}_4\text{depy}$  derivatives **[1]**( $\text{ClO}_4$ )<sub>2</sub> and **[2]**( $\text{ClO}_4$ )<sub>2</sub>, respectively, show that the Co-N bond distances in **2** were comparable to or shorter than those in **1**. The average Co-N<sub>eq</sub> for **2** is 2.097(2) Å, which is 0.062 Å shorter than the average value of 2.159(2) Å measured for **1**; average distances for the axial ligated atoms in each complex are more comparable at 2.067(2) Å and 2.059(2) Å for **2** and **1**, respectively. The steric constraints imposed by having three

heterocyclic rings conjoined by metal and  $sp^3$ -carbon anchors are typically manifest in an increase in the average magnitude of  $MN_{pz}-N_{pz}C_{methine}$  and  $MN_{py}-CC_{methine}$  torsion angles, or ‘ring-twist’ angles, where an unstrained system would be characterized by an average ring-twist angle of  $0^\circ$ .<sup>25</sup> The average torsion angles for **1** and **2** were found to be  $9.0^\circ$  and  $2.0^\circ$ , respectively. The lesser ring twisting in **2** ensures that the central pyridyl ring is aligned orthogonal to the least-squares equatorial  $N_4$ -plane, whereas the angle between the corresponding planes in the PY5 derivative is about  $21^\circ$  (Figure 3-3). The smaller steric profile of the five-membered pyrazolyl rings of  $pz_4depy$  also alleviates steric interactions at bridgehead metal and methine carbon atoms, while the smaller methyl group bound to the  $sp^3$ -carbon in  $pz_4depy$  versus the larger –OMe group of PY5 also likely contributes to the difference in ring-twisting.

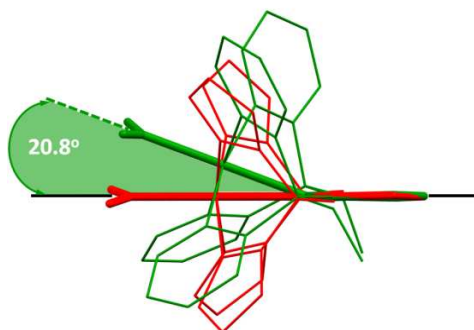


**Figure 3-3.** Comparison of dicationic structures of **1** (green) and **2** (red) where atoms of axial pyridine rings are overlaid to highlight the more idealized octahedral geometry of **2**. (Reproduced from Reference 11.)

This conjecture is supported by analysis of the structure of a related cobalt complex,  $[Co(PY5-Me_2)(H_2O)](OTf)_2$ , which has methyl groups rather than methoxy groups bound to the methine and shows a ring twist of  $8^\circ$ ; the remaining metrics are also between those of **1** and **2**:  $V_{oct} = 12.474 \text{ \AA}^3$ , Q.E. = 1.011, B.A.V. =  $38.24 \text{ deg}^2$ , avg.  $Co-N_{eq} = 2.139(2) \text{ \AA}$ .<sup>26</sup> While there is evidence that other metal complexes of PY5 are dynamic in solution and exist in overall  $C_2$  symmetry, the calculations demonstrate a clear preference for the bent geometry in gas-phase PY5 complexes. The importance of axial ligands in modulating the  $\sigma$ -donation into the  $d_z^2$  orbital helps govern reactivity in metal-aqua/hydroxo/oxo fragment of molecules of this type.<sup>27-29</sup> In

geometry-optimized (M06/Def2-SV(P)) complexes (free from packing effects), complexes of the pz<sub>4</sub>depy ligand were also found to have shorter metal-ligand bonds and a less distorted ligand framework than complexes of PY5 (Table 3-2).

The shorter distances (and lesser ring twisting) in pz<sub>4</sub>depy complexes versus PY5 complexes tends to increase overlap between ligand and metal orbitals and causes a destabilization of metal-centered occupied orbitals. Views of the highest occupied molecular orbitals of [(L)Co<sup>III</sup>(OH)]<sup>2+</sup> and [(L)Co<sup>II</sup>(OH)]<sup>+</sup> are given in Figure 3-4.

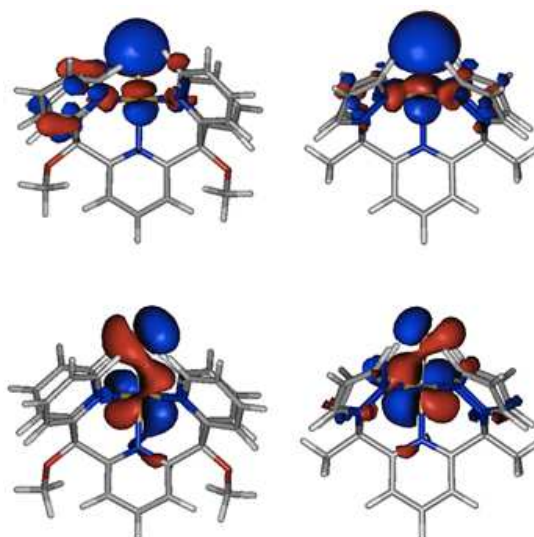


**Figure 3-4.**  $\beta$ -HOMOs of [(L)Co<sup>II</sup>(OH)]<sup>+</sup> (bottom) and HOMO of [(L)Co<sup>III</sup>(OH)]<sup>2+</sup> (top) for L = PY5 (left) and pz<sub>4</sub>depy (right). (Reproduced from Reference 11.)

In these complexes, the HOMO is a  $\pi^*$  orbital from the d  $\pi$  - p  $\pi$  interaction of the Co-O moiety. In each case, the orbital of pz<sub>4</sub>depy is higher energy than that of PY5, which gives rise to higher basicity of the former complexes. Coincidentally, the O-H bond in PY5 complexes is calculated to be slightly weaker than in the corresponding bond in pz<sub>4</sub>depy complexes (Figure 3-5 and Tables 3-3 through 3-6). The higher energy of the ( $\beta$ -) HOMOs and more electron-rich nature of cobalt(II) complexes of pz<sub>4</sub>depy versus PY5 results in a lower oxidation potential calculated for the former.



	L = PY5	L= pz <sub>4</sub> depy
[LCo(H <sub>2</sub> O)] <sup>2+</sup>	0	0
[LCo(H <sub>2</sub> O)] <sup>3+</sup>	138.788	132.819
[LCo(OH)] <sup>+</sup> + H <sup>+</sup>	171.672	174.804
[LCo(OH)] <sup>2+</sup> + H <sup>+</sup>	282.224	281.004

**Table 3-4.** Free energy (kcal/mol) of each species in Figure 3-5.

	H <sup>+</sup>	L = PY5			
		(L)Co <sup>II</sup> (H <sub>2</sub> O)	(L)Co <sup>III</sup> (H <sub>2</sub> O)	(L)Co <sup>II</sup> (OH)	(L)Co <sup>III</sup> (OH)
E <sub>SCF</sub> (hartree)	-0.164564	-3000.75073	-3000.538644	-3000.29184	-3000.123156
E <sub>SCF</sub> (kcal/mol)	-103.2653911	-1882998.09	-1882865.004	-1882710.132	-1882604.281
E <sub>SCF</sub> (eV)	-4.477901635	-81652.52789	-81646.75688	-81640.04117	-81635.45116
E+ZPE	-0.163147	-3000.234691	-3000.018283	-2999.788765	-2999.615537
H (hartree)	-0.162203	-3000.201493	-2999.986654	-2999.756903	-2999.584502
G (hartree)	-0.174563	-3000.296442	-3000.075269	-2999.848302	-2999.672126
G (kcal/mol)	-109.5398536	-1882713.02	-1882574.232	-1882431.808	-1882321.256
G (eV)	-4.749981424	-81640.16639	-81634.14812	-81627.97219	-81623.17832

**Table 3-5.** Summary of SCF energies and thermochemical data from theoretical calculations for (L)Co<sup>n+</sup>(OH<sub>x</sub>) where L=PY5. (M06/Def2-SV(P)).

	L = pz <sub>4</sub> depy			
	(L)Co <sup>II</sup> (H <sub>2</sub> O)	(L)Co <sup>III</sup> (H <sub>2</sub> O)	(L)Co <sup>II</sup> (OH)	(L)Co <sup>III</sup> (OH)
E <sub>SCF</sub> (hartree)	-2762.349408	-2762.147122	-2761.884089	-2761.723628
E <sub>SCF</sub> (kcal/mol)	-1733399.115	-1733272.178	-1733107.123	-1733006.432
E <sub>SCF</sub> (eV)	-75165.46104	-75159.95669	-75152.79938	-75148.43312
E+ZPE	-2761.911796	-2761.70565	-2761.45842	-2761.294565
H (hartree)	-2761.884024	-2761.679828	-2761.43142	-2761.269169
G (hartree)	-2761.967829	-2761.756168	-2761.514698	-2761.345457
G (kcal/mol)	-1733159.67	-1733026.851	-1732875.327	-1732769.126
G (eV)	-75155.078	-75149.31856	-75142.74799	-75138.14283

**Table 3-6.** Summary of SCF energies and thermochemical data from theoretical calculations for (L)Co<sup>n+</sup>(OH<sub>x</sub>) where L= pz<sub>4</sub>depy. (M06/Def2-SV(P)).

<i>Distances (Å)</i>	L = PY5				L = pz <sub>4</sub> depy			
	LCo(H <sub>2</sub> O)] <sup>2+</sup>	LCo(OH)] <sup>+</sup>	LCo(H <sub>2</sub> O)] <sup>3+</sup>	LCo(OH)] <sup>2+</sup>	LCo(H <sub>2</sub> O)] <sup>2+</sup>	LCo(OH)] <sup>+</sup>	LCo(H <sub>2</sub> O)] <sup>3+</sup>	LCo(OH)] <sup>2+</sup>
Co-O	2.072	1.888	1.956	1.841	2.053	1.881	1.942	1.834
Co-N <sub>py</sub>	2.086	2.183	1.931	1.994	2.136	2.254	1.924	1.988
Co-N <sub>eq</sub>	2.209	2.260	2.037	2.021	2.111	2.144	1.937	1.932
Co-N <sub>eq</sub>	2.208	2.227	2.029	2.017	2.111	2.140	1.933	1.931
Co-N <sub>eq</sub>	2.132	2.158	1.987	1.975	2.11	2.139	1.933	1.931
Co-N <sub>eq</sub>	2.131	2.156	1.984	1.969	2.109	2.136	1.928	1.927
avg. Co-N <sub>ax</sub> O	2.079	2.036	1.944	1.918	2.095	2.068	1.933	1.911
avg. Co-N <sub>eq</sub>	2.170	2.200	2.009	1.996	2.110	2.140	1.933	1.930
avg. Co-N <sub>all</sub>	2.153	2.197	1.994	1.995	2.115	2.163	1.931	1.942
avg. Co-N <sub>5</sub> O	2.140	2.145	1.987	1.970	2.105	2.116	1.933	1.924
<i>Angles (°)</i>								
C <sub>p</sub> -N <sub>py</sub> -Co <sup>a</sup>	152.9	147.8	163.5	161.6	175.8	173.5	180.0	179.5
avg. ring twist <sup>b</sup>	8.5	11.0	7.0	8.2	4.0	6.2	1.5	2.7
<sup>mp</sup> in <sub>py</sub> - <sup>mp</sup> in <sub>N<sub>4</sub></sub> <sup>c</sup>	63.1	58.5	72.5	70.8	85.7	83.5	90.0	89.5

**Table 3-7.** Main structural features in (M06/Def2-SV(P)) geometry- optimized [(L)Co(OH<sub>x</sub>)]<sup>z</sup> ions. <sup>a</sup> Cp = carbon *para*- to N on axial pyridine ring; <sup>b</sup> defined as the absolute value of C<sub>methine</sub>N<sub>pz</sub>-N<sub>pz</sub>Co or C<sub>methine</sub>C<sub>py</sub>-N<sub>py</sub>Co torsion angle (six such angles per complex); <sup>c</sup> dihedral angle between mean plane of the axial pyridyl ring and the mean plane of the four equatorial cobalt-bound nitrogen atoms.

Pourbaix diagrams for **1** and **2** were constructed by plotting pH versus the formal reduction potentials ( $E^0$ ) of the  $\text{Co}^{\text{III}}/\text{Co}^{\text{II}}$  redox couple, found using cyclic voltammetry. According to the Nernst equation, a one-electron one-proton process will give a 59 mV/pH slope on such a plot. The slope for  $[\text{Co}(\text{H}_2\text{O})\text{pz}_4\text{depy}]^{2+}$  (**1**) is 52 mV/pH, which is close enough (12% difference) that it can be assigned to a PCET event. Similar behavior is observed for  $[\text{Co}(\text{H}_2\text{O})\text{PY5}]^{2+}$  (**2**), which has a slope of 56 mV/pH on the Pourbaix diagram (see Figure 3-5).

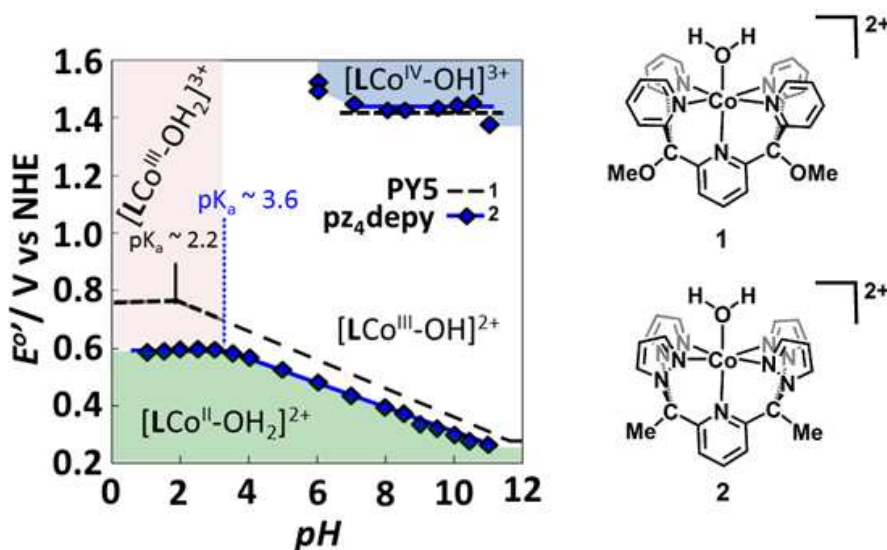
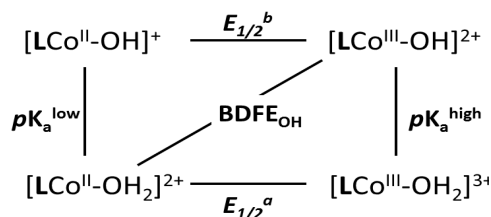


**Figure 3-5.** Comparison of Pourbaix diagrams of  $[(\text{PY5})\text{Co}(\text{OH}_2)]^{2+}$ , **1** versus  $[(\text{pz}_4\text{depy})\text{Co}(\text{OH}_2)]^{2+}$ , **2**.

The overall shorter Co-N bond distances and more ideal octahedral geometry about the metal center in **2** versus **1** gives rise to a more electron-rich  $\text{Co}^{\text{II}}(\text{H}_2\text{O})$  center and a more favorable  $[\text{LCo}^{\text{II}}(\text{H}_2\text{O})]/[\text{LCo}^{\text{III}}(\text{OH})]$  redox couple compared to **1**, as indicated by the anodic shift in the first oxidation. Also, from the onset of the pH dependence of the oxidation over the pH range 2-11 (solubility issues precluded determinations at higher pH) the  $\text{pK}_a$  of **2** of 3.6 is about 1.4 units higher (25 times more basic) than the PY5 complex, **1**. The more basic character of **2** versus **1** might be attributed to the lower stability of  $[\text{LCo}^{\text{II}}(\text{OH})]$  in the former versus the latter. These results demonstrate that seemingly subtle variations in the pentadentate ligand scaffold can lead to significant changes in the reactivity of the resulting complexes, which further justifies

the continued exploration into this area of chemistry. Scheme 3-1 gives the experimentally determined thermodynamic square-scheme associated with the PCET event for **1** and **2**.



**Scheme 3-2.** Thermodynamic square-scheme cycle used to calculate the bond dissociation free energy (BDFE) associated with the  $[\text{LCo}^{\text{II}}(\text{H}_2\text{O})]/[\text{LCo}^{\text{III}}(\text{OH})]^{2+}$  event.

An estimate of the O-H bond dissociation free energy can be made from the well-known relation of equation (1):<sup>30</sup>

$$\text{BDFE}(\text{OH}) = 23.06 E_{1/2} + 1.37 \text{ pK}_a + C \quad (\text{Eq. 3-1})$$

The constant C accounts for the free energy of solvation for  $\text{H}^\bullet$  in the chosen solvent. From Eq. 3-1 and the data summarized in the Pourbaix diagram of Fig. 3-5, the BDFE(OH) of **2** is estimated to be 76.7 kcal/mol whereas that for **1** is 71.6 kcal/mol. In other words, the hydroxocobalt(III) complex with the pz<sub>4</sub>depy ligand offers an additional 5 kcal/mol of driving force for C-H activation reactions compared to the related PY5 complex. It is also noteworthy that these values are on par with those calculated for  $[(\text{PY5})\text{M}(\text{H}_2\text{O})]^{2+}$  that show remarkable C-H activation chemistry (for M = Fe, BDE(OH) = 80 kcal/mol; for M = Mn, BDE(OH) = 82 kcal/mol).<sup>31</sup> Also, it is noteworthy that we previously found that the  $\text{Fe}^{2+}/\text{Fe}^{3+}$  couple can be tuned 0.2 V by simply changing from pz<sub>4</sub>lut to pz<sub>4</sub><sup>4Me</sup>lut in iron complexes. By extension, and in accord with Eq. 3-1, it is expected that a similar ligand substitution in cobalt complexes would attenuate the BDE(OH) by ca. 5 kcal/mol. We will examine the limits of this attenuation in future chemistry along with various C-H activation reactions.

Preliminary investigations of the high potential event of Figure 3-5 showed that cobalt complexes of our new ligand showed activity for electrochemical water oxidation as in Figure 3-6. Here, there is an enhanced catalytic current for water oxidation at about 1.4 V vs NHE. Accordingly, oxygen evolution was detected in the head space above the electrochemical set-up.

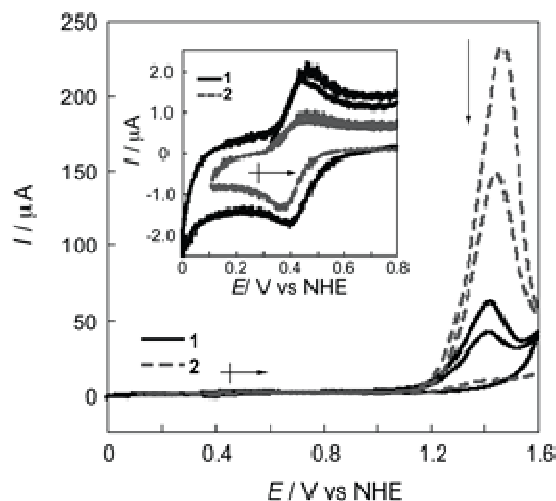


**Figure 3-6.** Cyclic voltammograms of **1** and **2** (0.5 mM) recorded in 0.1 M  $\text{KP}_i$  buffer (pH 9.2,  $n = 10 \text{ mV} \cdot \text{s}^{-1}$ ) demonstrating the enhanced catalytic currents associated with **2**.

Unfortunately, there was evidence for nanoparticle formation in highly basic solutions. Thus, the catalytic activity may be due to nano-particulate  $\text{CoO}_x$  species rather than being solely molecular in nature. Further studies are underway to determine the nature of the catalytically active species in these solutions.

Curtis Berlinguette and coworkers determined the catalytic cycle of  $[\text{Co}^{\text{II}}(\text{H}_2\text{O})\text{PY5}]^{2+}$ , as shown below.<sup>32</sup> This particular mechanism is a water nucleophilic attack mechanism. The other type of mechanism for water oxidation catalysts is a radical coupling mechanism. Three out of five species in the catalytic cycle appear on the Pourbaix diagram. Therefore, only part of the mechanism has been studied.

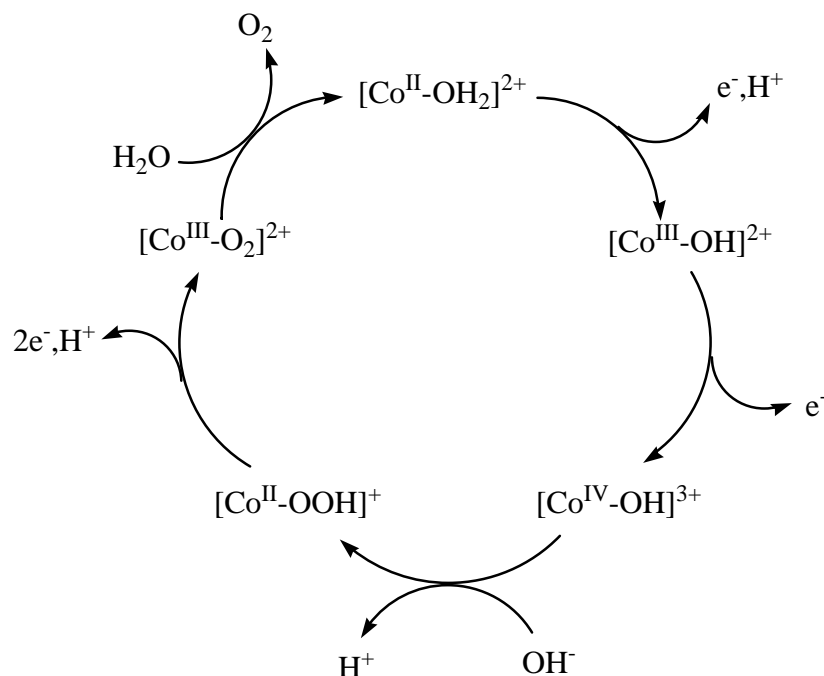


**Figure 3-7.** Catalytic Cycle of  $\text{Co}^{\text{II}}(\text{PY5})(\text{H}_2\text{O})]^{2+}$ , reproduced from Reference 32.

### 3-6 Conclusions:

The yield of the pentadentate ligand  $\text{pz}_4\text{depy}$  has been improved by using an easily-handled base  $\text{K}^t\text{BuO}$  to deprotonate  $\text{pz}_4\text{depy}$ . It has also been shown that replacing the equatorial pyridyl groups with pyrazolyl groups in PY5 to make  $\text{pz}_4\text{lut}$  changes the electrochemical properties of a corresponding transition metal complex dramatically. Water soluble aquacobalt(II) complexes were prepared and structurally characterized. The lower steric demands about the methine carbon of  $\text{pz}_4\text{depy}$  versus PY5 have been experimentally and theoretically verified. One result of the lower steric demands is that the  $\text{pz}_4\text{depy}$  ligand is less distorted than PY5 and can more favorably interact with the metal center, giving a slightly stronger ligand field than expected based on the relative donor capacities of pyridyl versus pyrazolyl groups. This subtle effect has a detectable impact on the electrochemistry of the complexes. Importantly, this study further demonstrates the kinetic stability afforded by pentadentate ligands, which allows for the study of proton coupled electron transfer reactions at a first-row transition metal center, in these current cases, PCET chemistry associated with the

oxidation of the  $[\text{Co-OH}_2]^{2+}$  unit. A PCET electrochemical analysis of this type has, to date, been confined primarily to a related osmium complex.<sup>34</sup> The changes in  $E_{1/2}$ ,  $pK_a$  and hence BDFE(OH) of the  $[\text{Co-OH}_2]^{2+}$  unit using different pentadentate ligands may be useful for the discovery of new C-H activation reactions.

## Chapter 4: Conclusions and Outlook

### 4-1 Conclusions:

Two new ligands, pz<sub>4</sub>depy and pz<sub>4</sub><sup>4Me</sup>depy, have been synthesized and their properties when coordinated to Fe<sup>II</sup> and Co<sup>II</sup> have been studied. An improved synthesis of pz<sub>4</sub>depy was also developed. The ease of deprotonating the pz<sub>4</sub>lut methine opens up a vast number of possible new molecules to further study the effects of adding different substituents to the sides of the ligand.

A series of [LFe<sup>II</sup>Cl]<sup>+</sup> complexes has been synthesized and their electronic and structural properties and ligand field strengths compared. By adding methyl groups to various positions along the ligand periphery, it was found that the 4-position on the pyrazole groups controls electronic effects, and the 3-position controls steric effects. Adding a methyl group to each methine carbon increased the ligand field strength.

One aquocobalt complex derived from complexation with pz<sub>4</sub>depy was found to be capable of water oxidation via a concerted PCET mechanism. This demonstrated the utility of pentadentate ligands as stabilizers for catalysts in a variety of reactions. When compared to PY5, pz<sub>4</sub>depy is a better donor to the metal center for a number of reasons. The cobalt(II) aqua complex has higher-energy HOMO's according to DFT calculations, which lead to a more basic O-H bond. This added basicity is proven by the higher pK<sub>a</sub> of 3.6, making it 25 times more basic than the PY5 analog. The pz<sub>4</sub>depy ligand is also more electron-rich, which results in a lower oxidation potential. The complex also has shorter Co-N bond distances and a more idealized octahedral geometry, which leads to a more electron-rich Co<sup>II</sup>(H<sub>2</sub>O) center and a more favorable [LCo<sup>II</sup>(H<sub>2</sub>O)]/[LCo<sup>III</sup>(OH)] redox couple. All of these factors contribute to a more favorable water oxidation pathway for this new catalyst.

### 4-2 Future directions:

The PY5 ligand has been shown to support Fe(III) complexes with an O-H bond that can activate relatively strong C-H bonds.<sup>Ref</sup> When [Fe<sup>III</sup>(PY5)(OH)]<sup>2+</sup> is reduced to [Fe<sup>II</sup>(PY5)(H<sub>2</sub>O)]<sup>2+</sup>,



hydrocarbons with C-H bond dissociation enthalpies less than 88 kcal/mol can be oxidized.<sup>1</sup> If the  $BDE_{OH}$  of  $[Fe^{III}(pz_4depy)(H_2O)]^{3+}$  follows the same trend as that of  $[Co^{II}(pz_4depy)(H_2O)]^{2+}$  ( $BDE(OH)=76.7$  kcal/mol, 5 kcal/mol higher than that of  $[Co^{II}(PY5)(H_2O)]^{2+}$ ), then this complex could be synthesized and oxidize hydrocarbons with  $BDE_{CH}$  values up to 5 kcal/mol greater than 88 kcal/mol. Assuming that the strongest C-H bond that this complex would be capable of oxidizing is 93 kcal/mol, some examples of hydrocarbons that could be oxidized are listed in Table 4-1.

Substrate	Predicted Product	$BDE(CH)$ (kcal/mol)
Benzaldehyde	Benzoic acid	74
Formaldehyde	Formic acid	76
Triphenylmethane	Triphenylmethanol	82
Toluene	Benzyl alcohol	85
Acetaldehyde	Acetic acid	88
Methanol	Methandiol	92
Acetone	1-hydroxy-2-propanone	92

**Table 4-1.** Predicted oxidation reactions of C-H bonds with  $[Fe^{III}pz_4depy(H_2O)]^{3+}$  as catalyst.<sup>2,3</sup>

One way to increase the  $BDE(OH)$  of the complex even more is to make it more basic by adding a negative charge to the ligand. For example, adding a  $SO_3^-$  group to the central pyridine would raise the maximum  $BDE(CH)$  to a value higher than 93 kcal/mol. There are a multitude of other ways to tune the strength of the CH bond that a complex in this series is capable of activating.

Another experiment could be performed to clarify a question raised in Chapter 2. Figure 2-7 shows the results of a temperature-dependent experiment to determine the change in magnetic moment of complexes **5** and **6**. An analogous temperature-dependent experiment could be performed by taking a UV-vis-NIR spectrum at multiple temperatures. This would show how the coordination of the complexes change with temperature, if at all.

## REFERENCES

## Chapter 1:

1. Alfred Werner - Biographical. [www.nobelprize.org/nobel\\_prizes/chemistry/laureates/1913/werner-bio.html](http://www.nobelprize.org/nobel_prizes/chemistry/laureates/1913/werner-bio.html) (accessed June 27, 2013), from Nobel Lectures, Chemistry 1901-1921, Elsevier Publishing Company, Amsterdam, 1966.
2. Spingler, B.; Scanavy-Grigorieff, M.; Werner, A.; Berke, H.; Lippard, S. J. *Inorg. Chem.* **2001**, *40*, 1065-1066.
3. Vaska, L. *Acc. Chem. Res.* **1976**, *9*, 175-183.
4. Sykes, A. G.; Weil, J. A. *Prog. Inorg. Chem.* **1970**, *13*, 1-106.
5. Kartha, G. *Acc. Chem. Res.* **1968**, *1*, 374-381.
6. Park, S.-Y.; Yokoyama, Y.; Shibayama, N.; Shiro, Y.; Tame, J. R. H. *J. Molec. Biol.* **2006**, *360*, 690-701.
7. Kendrew, J. C.; Dickerson, R. E.; Strandberg, B. E.; Hart, R. G.; Daview, D. R.; Phillips, D. C.; Shore, V. C. *Nature* **1960**, *185*, 422-427.
8. High-resolution Crystal Structures of Cobalamins in Vitamin B12 and B12-Proteins; B. Kräutler, D. Arigoni & B.T. Golding, Eds; Wiley-VCH, Weinheim, BRD: **1999**, 335-347.
9. Umena, Y.; Kawakami, K.; Shen, J.-R.; Kamiya, N. *Nature* **2011**, *473*, 55-60.
10. Lawrance, G. A. *Introduction to Coordination Chemistry*, John Wiley & Sons: West Sussex; 2010, 135.
11. Gispert, J. R. *Coordination Chemistry*, Wiley-VCH: Weinheim; 2008, 210.
12. Timmons, J. H.; Martell, A. H.; Harris, W. R.; Murase, I. *Inorg. Chem.* **1982**, *21*, 1525-1529.
13. Grohmann, A. *Dalton Trans.* **2010**, *39*, 1432-1440.
14. Karunadasa, H. I.; Chang, C. J.; Long, J. R. *Nature*, **2010**, *464*, 1329-1333.
15. Sun, Y.; Bigi, J. P.; Piro, N. A.; Tang, M. L.; Long, J. R.; Chang, C. J. *J. Am. Chem. Soc.* **2011**, *133*, 9212-9215.
16. Siedler-Egdal, R. K.; Nielsen, A.; Bond, A. D.; Bjerrum, M. J.; McKenzie, C. J. *Dalton Trans.* **2011**, *40*, 3849-3858.
17. Wasylenko, D. J.; Ganesamoorthy, C.; Borau-Garcia, J.; Berlinguette, C. P. *Chem. Commun.*, **2011**, *47*, 4249-4251.
18. Borovik, A. H. *Chem. Soc. Rev.*, **2011**, *40*, 1870-1874.
19. Kaizer, J.; Klinker, E. J.; Oh, N. Y.; Rohde, J.; Song, W. J.; Stubna, A.; Kim, J.; Munck, E.; Nam, W.; Que, Jr., L. *J. Am. Chem. Soc.* **2004**, *126*, 472-473.
20. Goldsmith, C. R.; Jonas, R. T.; Stack, D. P. *J. Am. Chem. Soc.* **2002**, *1*, 83-96.

21. Draksharapu, A.; Li, Q.; Roelfes, G.; Browne, W. R. *Dalton Trans.* **2012**, *41*, 13180-13190.
22. Kumar, P.; Kalita, A.; Mondal, B. *Dalton Trans.* **2013**, *42*, 5731-5739.
23. Wang, D.; Ray, K.; Collins, M. J.; Farquhar, E. R.; Frisch, J. R.; Gómez, L.; Jackson T. A.; Kerscher, M.; Waleska, A.; Comba, P.; Costas, M.; Que Jr., L. *Chem Sci.* **2013**, *4*, 282-291.
24. Rowland, J. M.; Olmstead, M.; Mascharak, P. K. *Inorg. Chem.* **2001**, *40*, 2810-2817.
25. Cho, J.; Jeon, S.; Wilson, S. A.; Liu, L. V.; Kang, E. A.; Braymer, J. J.; Lim, M. H.; Hedman, B.; Hodgson, K. O.; Valentine, J. S.; Solomon, E. I.; Nam, W. *Nature* **2011**, *478*, 502-505.
26. Prakash, J.; Kodanko, J. J. *Inorg. Chem.* **2012**, *51*, 2689-2698.
27. Morin, T. J.; Bennett, B.; Lindeman, S. V.; Gardinier, J. R. *Inorg. Chem.* **2008**, *47*, 7468-7470.
28. Morin, T. J.; Merkel, A.; Lindeman, S. V.; Gardinier, J. R. *Inorg. Chem.* **2010**, *49*, 7992-8002.

## Chapter 2:

1. Grohmann, A. *Adv. Inorg. Chem.* **2004**, *56*, 179-210.
2. Goldsmith, C. R.; Stack, T. D. P. *Inorg. Chem.* **2006**, *45*, 6048-6055.
3. De Vries, M. E.; La Crois, R. M.; Roelfes, G.; Kooijman, H.; Spek, A. L.; Hage, R.; Feringa, B. L. *Chem. Commun.* **1997**, 1549-1550.
4. Wong, E. L.-W.; Fang, G.-S.; Che, C.-M.; Zhu, N. *Chem. Commun.* **2005**, 4578-4580.
5. Rudd, D. J.; Goldsmith, S. R.; Cole, A. P.; Stack, D. P.; Hodgson, K. O.; Hedman, B. *Inorg. Chem.* **2005**, *44*, 1221-1229.
6. Muller, R. N.; Van der Elst, L.; Laurent, S. J. *Am. Chem. Soc.* **2003**, *125*, 8405.
7. Kahn, O.; Martinez, C. J. *Science* **1998**, *279*, 44.
8. Smeigh, A. L.; Creelman, M.; Mathics, R. A.; McCuskar, J. K. *J. Am. Chem. Soc.* **2008**, *130*, 14105-14107.
9. Morin, T. J.; Bennett, B.; Lindeman, S. V.; Gardinier, J. R. *Inorg. Chem.* **2008**, *47*, 7468.
10. Morin, T. J.; Merkel, A.; Lindeman, S. V.; Gardinier, J. R. *Inorg. Chem.* **2010**, *49*, 7992.
11. Evans, D. F. J. *Chem. Soc.* **1959**, 2003.
12. Noviandri, I.; Brown, K. N.; Fleming, D. S.; Gulyas, P. T.; Lay, P. A.; Masters, A. F.; Phillips, L. J. *Phys. Chem. B* **1999**, *103*, 6713.
13. SMART APEX2 Version 2.1-4, SAINT+ Version 7.23a and SADABS Version 2004/1. Bruker Analytical Xray Systems, Inc., Madison, Wisconsin, USA, 2005.
14. Oxford Diffraction (2009). CrysAlis Pro. Version 1.171.33.55 Oxford Diffraction Ltd, Yarnton, Oxfordshire, England.

15. Sheldrick, G. M. *Acta Cryst.*, **2008**, A64, 112-122.
16. Reger, D. L.; Grattan, T. C.; Brown, K. J.; Little, C. A.; Lamba, J. J. S.; Rheingold, A. L.; Sommer, R. D. J. *Organomet. Chem.* 2000, 607, 120.
17. Reger, D. L.; Gardinier, J. R.; Elgin, J. D.; Smith, M. D.; Hautot, D.; Long, G. J.; Grandjean, F. *Inorg. Chem.*, 2006, 45, 8862.
18. Goldsmith, C. R.; Jonas, R. T.; Cole, A. P.; Stack, T. D. P. *Inorg. Chem.* 2002, 41, 4642.
19. Ingalls, R. *Phys. Rev.*, 1964, A133, 787.
20. Atamini, C.; El Hajj, F.; Benmansour, S.; Marchivie, M.; Triki, S.; Conan, S.; Patinec, V.; Handel, H.; Dupouy, G.; Gómez-García, C. J. *Coord. Chem. Rev.* 2010, 254, 1559.

### Chapter 3:

1. CRC Handbook of Chemistry and Physics, 80th ed.; Lide, D.R., Ed.; CRC Press: Boca Raton, FL, 1999; p. 5-18.
2. Surendrananth, Y.; Kanan M. W.; Nocera, D. G. *J. Am. Chem. Soc.* **2010**, 132, 16501-16509.
3. Kanan, M. W.; Yano, J.; Surendrananth, Y.; Dinca, M.; Yachandra V. K.; Nocera, D. G. *J. Am. Chem. Soc.*, **2010**, 132, 13692-13701.
4. Kanan, M. W.; Nocera, D. G. *Science*, **2008**, 321, 1072-1075.
5. Gerken, J. B.; McAlpin, J. G.; Chen, J. Y. C.; Rigsby, M. L.; Casey, W. H.; Britt, R. D.; Stahl, S. S. *J. Am. Chem. Soc.* **2011**, 133, 14431-14442.
6. Wasylenko, D. J.; Ganesamoorthy, C.; Borau-Garcia, J.; Berlinguette, C. P. *Chem. Commun.*, **2011**, 47, 4249-4251.
7. Zhang, G.; Chen, K.; Chen, H.; Yao, J.; Shaik, S. *Inorg. Chem.* **2013**, [Online early access]. DOI: 10.1021/ic3028644. Published Online: April 5, 2013. <http://pubs.acs.org/doi/full/10.1021/ic3028644> (accessed April 10, 2013).
8. See chart 1: Grotjahn, D. B.; Brown, D. B.; Martin, J. K.; Marelus, D. C.; Abadjian, M.-C.; Tran, H. N.; Kalyuzhny, G.; Vecchio, K. S.; Specht, Z. G.; Cortes-Llamas, S. A.; Miranda-Soto, V.; van Niekerk, C.; Moore, C. E.; Rheingold, A. L. *J. Am. Chem. Soc.*, **2011**, 133, 19024-19027.
9. Farina, America; Hernandez, Sergio; Roman, Enrique. *J. Chem. Soc., Dalton Trans.*, **1989**, 849-851.
10. Wasylenko, D. J.; Palmer, R. D.; Schott, E.; Berlinguette, C. P. *Chem. Commun.*, **2012**, 48, 2107-2109.
11. Wasylenko, D. J.; Tatlock, H. M.; Bhandari, L. S.; Gardinier, J. R.; Berlinguette, C. P. *Chem. Sci.* **2013**, 4, 734.
12. Holmes, S. M.; McKinley, S. G.; Girolami, G. S.; Szalay, P. S.; Dunbar, K. R. *Inorg. Synth.* **2002**, 33, 91.

13. CrysAlisPro, Agilent Technologies, Version 1.171.34.46 (release 25-11-2010 CrysAlis171.NET), (compiled Nov. 25, 2010, 17:55:46).
14. Sheldrick, G. M. *Acta Cryst.*, **2008**, A64, 112-122.
15. SCALE3 ABSPACK – *An Oxford Diffraction program* (1.0.4,gui:1.0.3) © 2005 Oxford Diffraction Ltd.
16. Zhao, Y.; Truhlar, D. G. *Theor. Chem. Acc.* **2008**, 120, 215-241.
17. Weigend, F.; Ahlrichs, R. *Phys. Chem. Chem. Phys.* **2005**, 7, 3297-3305.
18. Scalmani G., Frisch, M. J. *J. Chem. Phys.* **2010**, 132, 114110-114124.
19. Gaussian 09, Revision B.01, Frisch, M. J.; Trucks, G. W.; Schlegel, H. B.; Scuseria, G. E.; Robb, M. A.; Cheeseman, J. R.; Scalmani, G.; Barone, V.; Mennucci, B.; Petersson, G. A.; Nakatsuji, H.; Caricato, M.; Li, X.; Hratchian, H. P.; Izmaylov, A. F.; Bloino, J.; Zheng, G.; Sonnenberg, J. L.; Hada, M.; Ehara, M.; Toyota, K.; Fukuda, R.; Hasegawa, J.; Ishida, M.; Nakajima, T.; Honda, Y.; Kitao, O.; Nakai, H.; Vreven, T.; Montgomery, Jr., J. A.; Peralta, J. E.; Ogliaro, F.; Bearpark, M.; Heyd, J. J.; Brothers, E.; Kudin, K. N.; Staroverov, V. N.; Kobayashi, R.; Normand, J.; Raghavachari, K.; Rendell, A.; Burant, J. C.; Iyengar, S. S.; Tomasi, J.; Cossi, M.; Rega, N.; Millam, J. M.; Klene, M.; Knox, J. E.; Cross, J. B.; Bakken, V.; Adamo, C.; Jaramillo, J.; Gomperts, R.; Stratmann, R. E.; Yazyev, O.; Austin, A. J.; Cammi, R.; Pomelli, C.; Ochterski, J. W.; Martin, R. L.; Morokuma, K.; Zakrzewski, V. G.; Voth, G. A.; Salvador, P.; Dannenberg, J. J.; Dapprich, S.; Daniels, A. D.; Farkas, Ö.; Foresman, J. B.; Ortiz, J. V.; Cioslowski, J.; Fox, D. J. Gaussian, Inc., Wallingford CT, 2009.
20. Becke, A. D. *J. Chem. Phys.* **1993**, 98, 5648-5652.
21. Lee, C.; Yang, W.; Parr, R. G. *Phys. Rev. B* **1988**, 37, 785-789.
22. Hay, P. J.; Wadt, W. R. *J. Chem. Phys.*, **1985**, 82, 270-283.
23. Wadt, W. R.; Hay, P. J. *J. Chem. Phys.*, **1985**, 82, 284-298.
24. Hay, P. J.; Wadt, W. R. *J. Chem. Phys.*, **1985**, 82, 299-310.
25. Reger, D. L.; Gardinier, J. R.; Elgin, J. D.; Smith, M. D. *Inorg. Chem.* **2006**, 45, 8862-8875.
26. see Sun, Y.; Bigi, J. P.; Piro, N. A.; Tang, M. L.; Long, J. R.; Chang, C. J. *J. Am. Chem. Soc.* **2011**, 133, 9212.
27. Hohenberger, J.; Ray K.; Meyer, K. *Nat. Commun.* **2012**, 3, 720.
28. Janardanan, D.; Usharani D.; Shaik, S. *Angew. Chem. Int. Ed.* **2012**, 51, 4421-4425.
29. Sastri, C. V.; Lee, J.; Oh, K.; Lee, Y. J.; Lee, J.; Jackson, T. A.; Ray, K.; Hirao, H.; Shin, W.; Halfen, J. A.; Kim, J.; Que Jr., L.; Shaik, S.; Nam, W. *Proc. Nat. Acad. Sci.* **2007**, 104, 19181-19186.
30. Warren, J. J.; Tronic, T. A.; Mayer, J. M. *Chem. Rev.* **2010**, 110, 6961-7001.
31. Goldsmith, C. R.; Stack, T. D. P. *Inorg. Chem.* **2006**, 45, 6048-6055.
32. Wasylenko, D. J.; Palmer, R. D.; Berlinguette, C. P. *Chem. Commun.* **2013**, 49, 218-227.

## Chapter 4:

1. Goldsmith, C. R.; Stack, T. D. P. *Inorg. Chem.* **2006**, *45*, 6048-6055.
2. Kaizer, J.; Klinker, E. J.; Oh, N. Y.; Rohde, J.-U.; Song, W. J.; Stubna, A.; Kim, J.; Münck, E.; Nam, W.; Que, Jr., L. *J. Am. Chem. Soc.* **2004**, *126*, 472-473.
3. Sanderson, R. T. *J. Am. Chem. Soc.* **1975**, *97*, 1367-1372.